

Continuous matrix product states for non-relativistic quantum fields: a lattice algorithm for inhomogeneous systems

Martin Ganahl* and Guifre Vidal

Perimeter Institute for Theoretical Physics, 31 Caroline Street North, Waterloo, ON N2L 2Y5, Canada

By combining the continuous matrix product state (cMPS) representation for quantum fields in the continuum with standard optimization techniques for matrix product states (MPS) on the lattice, we obtain an approximation $|\Psi\rangle$, directly in the continuum, of the ground state of non-relativistic quantum field theories. This construction works both for translation invariant systems and in the more challenging context of inhomogeneous systems, as we demonstrate for an interacting bosonic field in a periodic potential. Given the continuum Hamiltonian H , we consider a sequence of discretized Hamiltonians $\{H(\epsilon_\alpha)\}_{\alpha=1,2,\dots,p}$ on increasingly finer lattices with lattice spacing $\epsilon_1 > \epsilon_2 > \dots > \epsilon_p$. We first use energy minimization to optimize an MPS approximation $|\Psi(\epsilon_1)\rangle$ for the ground state of $H(\epsilon_1)$. Given the MPS $|\Psi(\epsilon_\alpha)\rangle$ optimized for the ground state of $H(\epsilon_\alpha)$, we use it to initialize the energy minimization for Hamiltonian $H(\epsilon_{\alpha+1})$, resulting in the optimized MPS $|\Psi(\epsilon_{\alpha+1})\rangle$. By iteration we produce an optimized MPS $|\Psi(\epsilon_p)\rangle$ for the ground state of $H(\epsilon_p)$, from which we finally extract the cMPS approximation $|\Psi\rangle$ for the ground state of H . Two key ingredients of our proposal are: (i) a procedure to discretize H into a lattice model where each site contains a two-dimensional vector space (spanned by vacuum $|0\rangle$ and one boson $|1\rangle$ states), and (ii) a procedure to map MPS representations from a coarser lattice to a finer lattice.

I. INTRODUCTION

Tensor networks for quantum lattice systems have their origins in the proposal twenty-five years ago of *matrix product states* (MPS)^{1–3} (introduced as finitely correlated states¹) and the advent of the density matrix renormalization group (DMRG)⁴. The tensor network formalism was later on generalized using concepts and tools from quantum information theory, leading to the proposal e.g. of the multi-scale entanglement renormalization ansatz (MERA)⁵ and projected entangled pair states (PEPS)⁶, and is nowadays the basis of powerful variational approaches to approximate the ground-state of local lattice Hamiltonians both in one and two spatial dimensions^{2,3}. This formalism can also be used to study quantum field theories (QFTs), after a suitable lattice discretization^{7–14}. More recently, important proposals were made to extend tensor networks from the lattice to the continuum, so that they can be applied to quantum fields directly –that is, without resorting to a lattice discretization. Prominent examples are the continuous MPS (cMPS)^{15,16} and the continuous MERA (cMERA)^{17–23}.

Ever since the original proposal of cMPS for non-relativistic QFTs in one spatial dimension by Verstraete and Cirac¹⁵, several optimization algorithms for ground-states of translation invariant systems have been put forward^{16,24–33} and applied to a number of systems. These include non-relativistic QFTs of interacting bosons^{24,25,27–29,32,33} and fermions^{26,30}, and even a relativistic QFT of fermions (after modifying the kinetic term at high energies)¹⁶. However, in inhomogeneous (that is, non-translation invariant) systems, the cMPS formalism has proven notoriously challenging and, besides important first steps²⁸, optimization algorithms have remained largely unaddressed. Only very recently, one of the authors has proposed a new, spline-based parametrization of inhomogeneous cMPS³³ and has shown how a ground-

state optimization for such states can be implemented.

A. Hybrid lattice/continuum strategy

In the present manuscript we propose a hybrid lattice/continuum strategy which combines lattice MPS optimization techniques with the cMPS representation. We use this strategy to produce a cMPS approximation $|\Psi\rangle$ to the ground-state of the continuum Hamiltonian H of an inhomogeneous QFT. Our central insight is that given a sufficiently fine lattice with spacing ϵ , and a discretized version $H(\epsilon)$ of a continuum Hamiltonian H , an MPS approximation $|\Psi(\epsilon)\rangle$ to the ground state of $H(\epsilon)$ already has a hidden cMPS structure. We make use of this hidden cMPS in two different ways: (1) We exploit the cMPS representation for continuum systems to relate two MPS representations on two lattices with different lattice spacing ϵ and ϵ' . Indeed, using rescaling properties of the cMPS representation, we can translate an optimized MPS $|\Psi(\epsilon)\rangle$ for $H(\epsilon)$ into an MPS $|\Psi'(\epsilon')\rangle$ on a lattice with lattice spacing $\epsilon' \neq \epsilon$. The state $|\Psi'(\epsilon')\rangle$ is of interest because it is already remarkably close to the ground-state of the Hamiltonian $H(\epsilon')$ on this second lattice, and thus provides an excellent starting point for an MPS energy minimization algorithm on that lattice. (2) Given the optimized MPS $|\Psi(\epsilon)\rangle$ for the ground-state of $H(\epsilon)$ for sufficiently small ϵ , we can extract its hidden cMPS structure and use it to directly build a cMPS approximation $|\Psi\rangle$ for the continuum Hamiltonian H . The resulting cMPS approximation $|\Psi\rangle$ for the ground-state of the QFT Hamiltonian H is seen to already be quite accurate. However, it is by no means an optimal cMPS approximation. Indeed, $|\Psi\rangle$ can be used as initialization of the recently introduced, spline-based, cMPS approach³³, which would then produce a better cMPS approximation.

A natural question arises: if we already have an inho-

mogeneous cMPS algorithm directly in the continuum³³, why should we then use the proposed hybrid MPS/cMPS algorithm at all? The answer is that cMPS algorithms are generally much more delicate than lattice MPS algorithms and work best starting from a sufficiently pre-converged cMPS. Indeed, as it is well documented³², even in the much better behaved case of translation invariant systems (both with euclidean time evolution³⁴ and energy minimization³² algorithms), a properly pre-converged cMPS is key to preventing fatal optimization instabilities and to very significantly improve convergence time.

We have mentioned above that the cMPS representation plays an important role not just in the continuum, but also in lattices approximating the continuum, since it provides a procedure to map wave-functions between lattices with different spacing ϵ and ϵ' . As a matter of fact, the cMPS representation has inspired a new scheme for discretizing a bosonic continuum Hamiltonian H . A standard discretization of H would lead to a boson Hubbard model where each site contains an infinite-dimensional complex vector space (corresponding to a bosonic degree of freedom). This vector space would be then truncated down to a d -dimensional complex vector space \mathbb{C}_d , with its d levels representing the vacuum (or no-boson) state $|0\rangle$ and n -boson states $|n\rangle$ for $n = 1, 2, \dots, d - 1$. The acceptable value of d on a given site might be hard to predict a priori and depends on the lattice spacing: at fixed particle density, the number of particles per site is proportional to ϵ and thus a coarser lattice requires a larger d than a finer lattice. The discretization scheme we propose in this manuscript produces instead a lattice where each site is described by a two-level complex vector space \mathbb{C}_2 , spanned by the vacuum state $|0\rangle$ and the one-boson state $|1\rangle$. In this case $H(\epsilon)$ can be thought of as a hard-core boson Hamiltonian with modified kinetic term. This has clear advantages over the standard discretization scheme. On the one hand, the same vector space dimension $d = 2$ independent of the lattice spacing ϵ avoids having to introduce a different MPS format (with tensors of different sizes) in changing from one lattice to another. On the other hand, the cost of MPS manipulations grows with the dimension of the local vector space, and therefore using the smallest possible dimension 2 leads to lower computational times.

B. Previous work on multigrid DMRG

Our algorithm belongs to the context of multigrid MPS approaches, as pioneered by M. Dolfi, B. Bauer, M. Troyer, and Z. Ristivojevic³⁵. In that work, a bosonic field on a periodic potential was also studied by first discretizing it onto a sequence of lattice Hamiltonians, and then sequentially finding an MPS approximation to the ground-state of each Hamiltonian, starting with the coarsest lattice and finishing with the finest one, and using the optimized MPS on one lattice to build an ini-

tial MPS for the optimization on the next, finer lattice. As the authors there demonstrated³⁵, a multi-grid MPS approach successfully circumvents the problem one faces when trying to directly optimize an MPS on the finest lattice, namely that the optimization gets stuck in local minima with an incorrect spatial profile of particle density. Our approach thus shares important similarities with this proposal. However, it also contains several significant improvements, based on exploiting the cMPS representation hidden in a lattice MPS, which we outline next.

On the one hand, while both approaches have as input a continuum Hamiltonian H , the multi-grid approach of Ref.³⁵ outputs an approximate ground-state wave-function on some fine lattice, whereas our hybrid algorithm outputs an approximate ground-state wave-function directly back in the continuum. This is not just a more natural format for the output (recall that the lattice was introduced only as a computational device), but one which may lead to easier comparison with other continuum approaches, such as perturbative methods³⁶, Bethe Ansatz^{37,38} or the Gross-Pitaevskii approach³⁹⁻⁴¹.

A second major difference is in how the transition from a coarser lattice to a finer lattice takes place in the two approaches. Dolfi et al.³⁵ use an ad hoc MPS splitting procedure that is essentially independent of the actual wave-function under consideration. Instead, by extracting and exploiting the approximate cMPS structure hidden in a lattice MPS, we will see that our approach produces a better pre-converged initial state on the finer lattice. In addition, the hidden cMPS description allows for much more flexibility in how the coarser and finer lattice relate. While the method proposed by Dolfi et al.³⁵ is restricted to mapping one site to n sites, here we can map m sites to n sites for any pair of integers m, n – and one can even consider transitions between two irregular lattice discretizations (where both coarser and finer lattices have a lattice spacing that depends on position). Such flexibility is relevant when studying inhomogeneous systems with e.g. a position-dependent potential $V(x)$ that changes faster in some places than others, since it allows us to locally adjust the lattice spacing to the needs of the problem.

Finally, a third important difference is that Dolfi et al.³⁵ used a standard scheme to discretize the continuum bosonic Hamiltonian H into a lattice Hamiltonian on a lattice where each site had a complex vector space truncated to $d = 3$ levels, whereas we propose and use a discretization scheme that produces $d = 2$ -level sites, and thus potentially smaller computational times.

C. Outline

The rest of the manuscript is organized into the following sections:

In Sect. II we review necessary background material, including standard discretization of a continuous Hamil-

tonian H into a lattice, and the cMPS and MPS variational states. In the remaining sections we present our proposed algorithm, together with a demonstration of its performance. More specifically, in Sect. III we explain how to extract a hidden, approximate cMPS representation from an MPS, and how to discretize a continuous, bosonic Hamiltonian H into a two-level lattice model. In Sect. IV we describe the algorithm that takes as input a continuum Hamiltonian H and produces a cMPS approximation $|\Psi\rangle$ for its ground-state, with technical details described in the Appendix. In Sect. V we present results for a concrete system, and in Sect. VI we compare our approach to the multi-grid method proposed by Dolfi et al.³⁵.

II. BACKGROUND MATERIAL

In this section we review the type of QFT Hamiltonian H whose ground-state we would like to investigate, its discretization onto a sequence of lattice Hamiltonians $H(\epsilon_\alpha)$, as well as the continuous MPS to approximate ground-states directly in the continuum and the matrix product state (MPS) to approximate ground-states of the lattice.

A. Hamiltonian in the continuum

For the sake of concreteness, in this manuscript we focus on a specific inhomogeneous Hamiltonian for a non-relativistic bosonic field of the form

$$H = \frac{1}{2m} \int dx \partial_x \psi^\dagger(x) \partial_x \psi(x) + \int dx \mu(x) \psi^\dagger(x) \psi(x) + g \int dx \psi^\dagger(x) \psi^\dagger(x) \psi(x) \psi(x), \quad (1)$$

which describes the dynamics of a single species of a bosonic field on the real line. The creation operator $\psi(x)$ fulfills the canonical bosonic field commutation relations

$$[\psi(x), \psi^\dagger(y)] = \delta(x - y). \quad (2)$$

Above, $\frac{1}{2m} \int dx \partial_x \psi^\dagger(x) \partial_x \psi(x)$ is the non-relativistic kinetic term, with m the mass of a boson, $g \int dx \psi^\dagger(x) \psi^\dagger(x) \psi(x) \psi(x)$ is a quartic local interaction term with interaction strength g and $\int dx \mu(x) \psi^\dagger(x) \psi(x)$ is a chemical potential term. In this work we will focus on the case of a periodic chemical potential of the form

$$\mu(x) = \mu_0 + V_0 \left(\cos\left(\frac{2\pi x}{L}\right) - 1 \right)^2 \quad (3)$$

parametrized by offset μ_0 , amplitude V_0 and periodicity L . More generally, one could consider a similar Hamiltonian involving multi-species of bosons, single species or multiple species of fermionic fields, and even a mixture of bosonic and fermionic fields.

B. Hamiltonian on the lattice

Hamiltonian H in Eq.(1) can be discretized following a standard procedure. First, the real line \mathbb{R} is replaced by a lattice $\mathcal{L}(\epsilon)$ of equidistant points $\{x_i \equiv \epsilon i\}_{i \in \mathbb{Z}}$, with lattice spacing $\epsilon \equiv x_{i+1} - x_i$. At each position x_i , one then replaces the bosonic annihilation operator $\psi(x)$ in the continuum with a bosonic annihilation operator $\psi(x_i)$ defined as

$$\psi(x) \rightarrow \psi(x_i) \equiv \frac{1}{\sqrt{\epsilon}} c_i. \quad (4)$$

c_i is a bosonic lattice annihilation operator at site i fulfilling the canonical bosonic lattice commutation relations

$$[c_i, c_j^\dagger] = \delta_{ij}. \quad (5)$$

Using the standard replacements $\int dx \rightarrow \epsilon \sum_i$ and $\partial_x f(x) \rightarrow (f(x + \epsilon) - f(x))/\epsilon$, the non-relativistic kinetic term becomes

$$\frac{1}{2m} \int dx \partial_x \psi^\dagger(x) \partial_x \psi(x) \rightarrow \quad (6)$$

$$- \frac{1}{2m\epsilon^2} \sum_i \left(c_i^\dagger c_{i+1} + h.c. \right) + \frac{1}{m\epsilon^2} \sum_i c_i^\dagger c_i, \quad (7)$$

whereas the chemical potential term transforms into

$$\int dx \mu(x) \psi^\dagger(x) \psi(x) \rightarrow \sum_i \mu_i c_i^\dagger c_i, \quad (8)$$

with $\mu_i \equiv \mu(x_i)$, and the interaction term reads

$$g \int dx \psi^\dagger(x) \psi^\dagger(x) \psi(x) \psi(x) \rightarrow \frac{g}{\epsilon} \sum_i c_i^\dagger c_i^\dagger c_i c_i. \quad (9)$$

We therefore end up with the lattice Hamiltonian

$$H(\epsilon) \equiv - \frac{1}{2m\epsilon^2} \sum_i \left(c_i^\dagger c_{i+1} + h.c. \right) + \sum_i \left(\mu_i + \frac{1}{m\epsilon^2} \right) c_i^\dagger c_i + \frac{g}{\epsilon} \sum_i c_i^\dagger c_i^\dagger c_i c_i. \quad (10)$$

We emphasize that later on we will propose a more convenient, alternative discretization scheme which results in modified kinetic and interaction terms, see Eq.(46), acting on a lattice $\mathcal{L}(\epsilon)$ where each site is described by a two-dimensional complex vector space spanned by $|0\rangle$ and $|1\rangle$, that is $d = 2$, for any value of ϵ .

Hamiltonian $H(\epsilon)$ acts on a lattice where each site i is described by an infinite-dimensional complex vector space spanned by states $\{|n_i\rangle\}$, for $n_i = 0, 1, 2, \dots$, where the state $|n_i\rangle$ fulfills $c_i^\dagger c_i |n_i\rangle = n_i |n_i\rangle$ and thus corresponds to having n_i bosonic particles on that site. In practical calculations one must truncate this basis to a finite number d of states, so that $n_i = 0, 1, \dots, d-1$. In a ground-state calculation, this approximation may be well justified (see below).

C. Scaling of expectation values with ϵ

Let us assume that the ground-state expectation value of the particle density $\langle n(x) \rangle \equiv \langle \psi^\dagger(x)\psi(x) \rangle$, the quartic term $\langle \psi^\dagger(x)\psi^\dagger(x)\psi(x)\psi(x) \rangle$, and the kinetic term $\langle \partial_x \psi^\dagger(x)\partial_x \psi(x) \rangle$ are finite and that the corresponding lattice expectation values converge smoothly to the continuum. This implies that, for small lattice spacing ϵ and to leading order in ϵ , we have

$$\langle c_i^\dagger c_i \rangle \approx \epsilon \langle \psi^\dagger(x)\psi(x) \rangle = O(\epsilon), \quad (11)$$

$$\langle c_i^\dagger c_i^\dagger c_i c_i \rangle \approx \epsilon^2 \langle \psi^\dagger(x)\psi^\dagger(x)\psi(x)\psi(x) \rangle = O(\epsilon^2), \quad (12)$$

$$\langle (c_{i+1} - c_i)^\dagger (c_{i+1} - c_i) \rangle \approx \epsilon^3 \langle \partial_x \psi^\dagger(x)\partial_x \psi(x) \rangle = O(\epsilon^3). \quad (13)$$

In particular, if $P_{n_i} \equiv \langle |n_i\rangle \langle n_i| \rangle$ is the probability that site i is found in state $|n_i\rangle$ when the lattice is in the ground-state of $H(\epsilon)$, with $\sum_{n_i} P_{n_i} = 1$ and $P_{n_i} \geq 0$, then we have $\langle c_i^\dagger c_i \rangle = \sum_{n_i} n_i P_{n_i}$, $\langle c_i^\dagger c_i^\dagger c_i c_i \rangle = \sum_{n_i} n_i(n_i - 1)P_{n_i}$ and Eqs. (11)-(12) imply

$$O(\epsilon) = \sum_{n_i=0}^{\infty} n_i P_{n_i} \geq \sum_{n_i=1}^{\infty} P_{n_i}, \quad (14)$$

$$O(\epsilon^2) = \sum_{n_i=0}^{\infty} n_i(n_i - 1)P_{n_i} \geq \sum_{n_i=2}^{\infty} P_{n_i}. \quad (15)$$

Eq.(14) tells us that the probability P_1 of finding one or more boson on one site is at most $O(\epsilon)$. Eq.(15) implies that the probability P_2 of finding two or more bosons at one site is at most $O(\epsilon^2)$. If we were to truncate the Hilbert space dimension to $d = 2$, then we would be throwing away contributions of order ϵ^2 . However, this approximation would be incompatible with the interaction term in the Hamiltonian Eq.(1), which requires at least two bosons on one site, that is $d = 3$. We conclude that a valid truncation of the local Hilbert space requires at least $d = 3$.

D. Continuous matrix product states

The continuous matrix product state (cMPS)^{15,42} is a variational ansatz for ground-states of non-relativistic QFT Hamiltonians such as H in Eq.(1). On the real line it has the form

$$|\Psi\rangle = v_l^\dagger \mathcal{P} e^{\int_{-\infty}^{\infty} dx Q(x) \otimes \mathbb{1} + R(x) \otimes \psi^\dagger(x)} v_r |0\rangle, \quad (16)$$

where for each value $x \in \mathbb{R}$, $Q(x), R(x) \in \mathbb{C}^{D \times D}$ are $D \times D$ matrices of complex coefficients, $\mathcal{P}e$ denotes a path ordered exponential, $|0\rangle$ is the physical vacuum, that is $\psi(x)|0\rangle = 0 \quad \forall x \in \mathbb{R}$, and v_l, v_r are arbitrary boundary vectors at $x = \pm\infty$.

The matrix functions $Q(x)$ and $R(x)$ contain the variational parameters of the ansatz. The expectation value

of local observables can be expressed in terms of these matrices. For instance, we have

$$\langle \psi^\dagger(x)\psi(x) \rangle = \langle l(x) | R(x) \otimes \bar{R}(x) | r(x) \rangle, \quad (17)$$

$$\langle \psi^\dagger(x)\psi^\dagger(x)\psi(x)\psi(x) \rangle = \langle l(x) | R^2(x) \otimes \bar{R}^2(x) | r(x) \rangle, \quad (18)$$

$$\langle \partial_x \psi^\dagger(x)\partial_x \psi(x) \rangle = \langle l(x) | \left([Q(x), R(x)] + \frac{dR(x)}{dx} \right) \otimes \left([\bar{Q}(x), \bar{R}(x)] + \frac{d\bar{R}(x)}{dx} \right) | r(x) \rangle, \quad (19)$$

where $\langle l(x) |$ and $| r(x) \rangle$ are D^2 -dimensional vectors that depend on the cMPS description at smaller and larger values of x , respectively, and fulfill $\langle l(x) | r(x) \rangle = \langle \Psi | \Psi \rangle = 1$. In particular, $\langle l(x) |$ and $| r(x) \rangle$ can be chosen to have only finite entries and therefore finite matrices $Q(x)$ and $R(x)$ and $dR(x)/dx$ will guarantee a finite value for Eqs. (17)-(19).

E. Lattice matrix product states

The MPS is a variational ansatz for ground-states of lattice Hamiltonians such as $H(\epsilon)$ in Eq.(10). It has the form

$$|\Psi\rangle = \sum_{\dots, n_i, n_{i+1}, \dots} \dots A_{n_i}^{[i]} A_{n_{i+1}}^{[i+1]} \dots | \dots n_i n_{i+1} \dots \rangle \quad (20)$$

where i labels lattice sites, and $n_i = 0, 1, \dots, d-1$ labels states $|n_i\rangle$ of the occupation number basis on that site. $A_{n_i}^{[i]} \in \mathbb{C}^{D \times D}$ is a $D \times D$ matrix of complex coefficients. We often refer to the set of d matrices $\{A_0^{[i]}, A_1^{[i]}, \dots, A_{d-1}^{[i]}\}$ on site i as a three-index MPS tensor and denote it as $A^{[i]}$.

The MPS tensors $A^{[i]}$ for all sites $i \in \mathbb{Z}$ contain the variational parameters of this ansatz.

F. Periodic potential

In this work we consider that the chemical potential $\mu(x)$ in the continuum Hamiltonian H in Eq.(1) is a periodic function,

$$\mu(x+L) = \mu(x). \quad (21)$$

We will then assume that the ground-state of H has the same periodicity, which we will incorporate into the cMPS through the periodicity conditions

$$Q(x+L) = Q(x), \quad R(x+L) = R(x). \quad (22)$$

By choosing a lattice spacing ϵ such that $L/\epsilon \equiv N \in \mathbb{N}$, the discretized Hamiltonian $H(\epsilon)$ in Eq.(10) is periodic under shifts by N sites, with the chemical potential μ_i fulfilling $\mu_{i+N} = \mu_i$. In that case, if the ground state is also periodic under shifts of N sites, we can restrict

out attention to an MPS with a unit cell consisting of N MPS tensors $\{A^{[i]}, A^{[i+1]}, \dots, A^{[i+N-1]}\}$, with

$$A^{[i+N]} = A^{[i]}. \quad (23)$$

Several results presented in the next sections do not rely on having a periodic potential.

G. cMPS as the continuous limit of an MPS

The cMPS wave function Eq.(16) can be understood¹⁵ as the continuum limit of a continuous family of MPS $A^{[i]}(\epsilon)$ parametrized by the lattice spacing ϵ of the lattice $\mathcal{L}(\epsilon)$ and defined as

$$A_0^{[i]}(\epsilon) \equiv \mathbb{1} + \epsilon Q(x_i) \quad n_i = 0, \quad (24)$$

$$A_{n_i}^{[i]}(\epsilon) \equiv \sqrt{\frac{\epsilon^{n_i}}{n_i!}} [R(x_i)]^{n_i} \quad n_i \geq 1, \quad (25)$$

where $Q(x_i)$ and $R(x_i)$ are the cMPS matrices $Q(x)$ and $R(x)$ evaluated at $x = x_i$. Indeed, in the limit $\epsilon \rightarrow 0$ one can recover the cMPS decomposition in Eq.(16) from the MPS decomposition in Eq.(20)¹⁵.

The particular form of the MPS tensors $A^{[i]}$ in Eq.(24)-Eq.(25) ensures that expectation values of local operators such as $\langle c_i^\dagger c_i \rangle$, $\langle c_i^\dagger c_i^\dagger c_i c_i \rangle$, and $\langle (c_{i+1} - c_i)^\dagger (c_{i+1} - c_i) \rangle$ are continuous as a function of the lattice spacing ϵ and scale as in Eqs. (11)-(13) for small values of ϵ .

H. Gauge freedom

The cMPS representation contains a gauge freedom, meaning that there are redundant parameters. If $Q(x), R(x)$ is a cMPS representing a state $|\Psi\rangle$, then the pair $\tilde{Q}(x)$ and $\tilde{R}(x)$ given by

$$\tilde{Q}(x) = g(x)Q(x)g(x)^{-1} - \frac{dg(x)}{dx}g(x)^{-1} \quad (26)$$

$$\tilde{R}(x) = g(x)R(x)g(x)^{-1} \quad (27)$$

is another cMPS that represents the same state $|\Psi\rangle$. Here $g(x)$ is some invertible $D \times D$ matrix. We can use this freedom to impose certain conditions on the cMPS matrices. In this work we will mostly work on the left canonical gauge, characterized by

$$Q^\dagger(x) + Q(x) + R^\dagger(x)R(x) = 0, \quad (28)$$

for which the D^2 -dimensional left vector $\langle l(x) |$ and right vector $|r(x)\rangle$ become the identity operator and a diagonal density matrix, after they are reorganized as $D \times D$ matrices.

Analogously, on the lattice the MPS representation $A^{[i]}$ and $\tilde{A}^{[i]}$ represent the same state $|\Psi\rangle$ if they are related by

$$\tilde{A}^{[i]} = g^{[i-1]}A^{[i]}(g^{[i]})^{-1}, \quad (29)$$

where, for all $i \in \mathbb{Z}$, the $D \times D$ matrix $g^{[i]}$ is invertible. The left canonical gauge reads

$$\sum_{n_i} (A_{n_i}^{[i]})^\dagger A_{n_i}^{[i]} = \mathbb{1}, \quad \sum_{n_i} A_{n_i}^{[i]} \rho (A_{n_i}^{[i]})^\dagger = \rho, \quad (30)$$

where ρ is a diagonal density matrix containing the squares of the Schmidt values λ_α , i.e.

$$[\rho]_{\alpha\beta} = \lambda_\alpha^2 \delta_{\alpha\beta}$$

III. EXPLOITING THE CMPS REPRESENTATION ON THE LATTICE

In this section we explain how to extract a cMPS representation from an MPS that approximates the ground-state on a fine lattice. We then propose a modified discretization scheme that produces discrete Hamiltonians $H(\epsilon)$ on a lattice made of two-level sites. Finally, we explain how to use the hidden cMPS representation to map an MPS on one lattice to an MPS on another lattice.

A. Extraction of a cMPS from a lattice MPS

Given a lattice MPS $|\Psi(\epsilon)\rangle$ that approximates the ground-state of $H(\epsilon)$, we extract cMPS matrices $Q(x)$ and $R(x)$ evaluated on the points $x_i \in \mathcal{L}(\epsilon)$ through

$$Q(x_i) \equiv \frac{A_0^{[i]} - \mathbb{1}}{\epsilon}, \quad (31)$$

$$R(x_i) \equiv \frac{A_1^{[i]}}{\sqrt{\epsilon}}, \quad (32)$$

and then extend these matrices $Q(x_i)$ and $R(x_i)$ from $\mathcal{L}(\epsilon)$ to the real line by interpolation (see below).

It is important to recognize that $Q(x_i)$ depends non-trivially on the choice of gauge in the MPS. Indeed, if $\tilde{A}^{[i]}$ relates to $A^{[i]}$ through Eq.(29), then it is easy to check that for $\tilde{Q}(x_i) \equiv (\tilde{A}_0^{[i]} - \mathbb{1})/\epsilon$ we get

$$\tilde{Q}(x_i) = \frac{1}{\epsilon} \left(g^{[i-1]} A^{[i]} (g^{[i]})^{-1} - \mathbb{1} \right) \quad (33)$$

$$\neq \frac{1}{\epsilon} g^{[i-1]} \left(A^{[i]} - \mathbb{1} \right) (g^{[i]})^{-1} \quad (34)$$

$$= g^{[i-1]} Q(x_i) (g^{[i]})^{-1} \quad (35)$$

which means that the final cMPS state $|\Psi\rangle$ extracted from the MPS state $|\Psi(\epsilon)\rangle$ is affected by the specific gauge choice we work with. In particular, a random choice of gauge may result in matrices $Q(x_i)$ and $R(x_i)$ that change abruptly with x_i . This typically leads to a cMPS that is not as useful for our current purposes. We have heuristically determined that it is best to work with a diagonal gauge, such as e.g. the left canonical gauge of Eq.(30), which we use from now on (see Appendix A

for a more detailed explanation). In particular, interpolation of the matrices $Q(x_i), R(x_i)$ is carried out in this diagonal gauge. To extend the extracted state to the continuum, we use a standard basis-spline interpolation on the matrix entries $[Q(x_i)]_{\alpha\beta}, [R(x_i)]_{\alpha\beta}$. For brevity, let $M \in \{Q, R\}$ label the two different matrices in the following. Each interpolation takes as input a set of data points $(x_i, [M(x_i)]_{\alpha\beta})$. A continuous and smooth function $f_{\alpha\beta}^M(x)$ is then constructed such that $f_{\alpha\beta}^M(x_i) \equiv [M(x_i)]_{\alpha\beta}$. The function $f_{\alpha\beta}^M(x)$ is chosen as an expansion in so-called order k basis-spline polynomials $B_i^k(x)$, i.e.

$$f_{\alpha\beta}^M(x) = \sum_i B_i^k(x) \mathcal{F}_{\alpha\beta}^{M,i} \quad (36)$$

with properly chosen expansion coefficients $\mathcal{F}_{\alpha\beta}^{M,i}$ ^{33,43}. The polynomials $B_i^k(x)$ have finite support on a small region inside the interval $[0, L]$, with L the periodicity of the Hamiltonian H . We use order $k = 5$ polynomials in this manuscript, and use periodic spline interpolation. The cMPS matrix functions are then given by

$$\begin{aligned} Q_{\alpha\beta}(x) &= f_{\alpha\beta}^Q(x) \\ R_{\alpha\beta}(x) &= f_{\alpha\beta}^R(x) \end{aligned}$$

The cMPS matrices $Q(x)$ and $R(x)$ extracted from an MPS are useful for a number of purposes. For instance, when working on a lattice $\mathcal{L}(\epsilon)$ with sufficiently small lattice spacing ϵ , the extracted cMPS may already provide a good approximation to the ground-state of the continuum Hamiltonian H .

B. Mapping an MPS from $\mathcal{L}(\epsilon)$ to $\mathcal{L}(\epsilon')$

On the other hand, we can use the extracted cMPS matrices $Q(x)$ and $R(x)$ and Eqs. (24)-(25) to define a new state $|\Psi'(\epsilon')\rangle$ on another lattice $\mathcal{L}(\epsilon')$ with lattice spacing $\epsilon' \neq \epsilon$, such that site i in $\mathcal{L}(\epsilon)$ and in $\mathcal{L}(\epsilon')$ is on positions x_i and x'_i , respectively, with

$$x_i \equiv \epsilon i, \quad x'_i \equiv \epsilon' i. \quad (37)$$

Indeed, we can define MPS tensors for $|\Psi'(\epsilon')\rangle$ according to

$$A_0^{[i]} \equiv \mathbb{1} + \epsilon' Q(x'_i) \quad n_i = 0, \quad (38)$$

$$A_{n_i}^{[i]} \equiv \sqrt{\frac{\epsilon'^{n_i}}{n_i!}} [R(x'_i)]^{n_i} \quad n_i \geq 1, \quad (39)$$

so that, overall, we map $|\Psi(\epsilon)\rangle$ into $|\Psi'(\epsilon')\rangle$ through three steps

$$A^{[i]} \xrightarrow{\text{Eqs. (31),(32)}} Q(x_i), R(x_i) \quad (40)$$

$$\xrightarrow{\text{interpolation}} Q(x), R(x) \quad (41)$$

$$\xrightarrow{\text{Eqs. (38),(39)}} A'^{[i]}. \quad (42)$$

C. Modified discretization

Recall that on the lattice we can truncate the infinite-dimensional vector space on each site down to d dimensions, where d depends on the lattice spacing ϵ . Recall also that the cost of an MPS computation grows with d , and therefore it would be convenient to work with the smallest non-trivial local space, which corresponds to $d = 2$. It would therefore be of interest if we could discretize the continuum Hamiltonian H into a lattice Hamiltonian $H(\epsilon)$ acting on a lattice where each site has a vector space of dimension $d = 2$. It turns out that by thinking in terms of the cMPS decomposition, this is possible.

To make a local Hilbert space dimension of $d = 2$ compatible with a bosonic theory, the discretized kinetic and interaction energy operators have to be modified. Let us first discuss the necessary modifications for the kinetic energy operator. For illustration purposes, let us for a moment consider a *translation invariant* MPS $|\Psi\rangle$ with tensors $A_{n_i}^{[i]}(\epsilon)$ of the form

$$\begin{aligned} A_0^{[i]}(\epsilon) &= \mathbb{1} + \epsilon Q & n_i = 0 \\ A_{n_i}^{[i]}(\epsilon) &= \sqrt{\frac{\epsilon^{n_i}}{n_i!}} [R]^{n_i} & n_i \geq 1. \end{aligned}$$

However, the following results are equally valid for an inhomogeneous state.

Let us recall that the action of the annihilation operator c_i on the state $|\Psi\rangle$ is given by

$$c_i |\Psi\rangle = \dots A_{n_{i-1}}^{[i-1]} \left[\sqrt{\epsilon} R |0\rangle + \mathcal{O}(\epsilon^{3/2}) \right] A_{n_{i+1}}^{[i+1]} \dots$$

If we compute the action of the discretized derivative operator $\frac{1}{\epsilon^{3/2}} (\mathbb{1}_i c_{i+1} - c_i \mathbb{1}_{i+1})$ on this state, we obtain, to lowest orders in ϵ , an expression of the form

$$\begin{aligned}
& \frac{1}{\epsilon^{3/2}} (\mathbb{1}_i c_{i+1} - c_i \mathbb{1}_{i+1}) |\Psi\rangle = \\
& \dots A_{n_{i-1}}^{[i-1]} \frac{1}{\epsilon^{3/2}} \left[(\mathbb{1} + \epsilon Q) \sqrt{\epsilon} R |00\rangle + (\mathbb{1} + \epsilon Q) \sqrt{\frac{\epsilon^2}{2}} \sqrt{2} R^2 |01\rangle + \epsilon R^2 |10\rangle \right. \\
& \quad \left. - \sqrt{\epsilon} R (\mathbb{1} + \epsilon Q) |00\rangle - \sqrt{\frac{\epsilon^2}{2}} \sqrt{2} R^2 (\mathbb{1} + \epsilon Q) |10\rangle - \epsilon R^2 |01\rangle + \mathcal{O}(\epsilon^2) \right] A_{n_{i+2}}^{[i+2]} \dots \\
& = \dots A_{n_{i-1}}^{[i-1]} \frac{1}{\epsilon^{3/2}} \left[\underbrace{\left((\mathbb{1} + \epsilon Q) \sqrt{\epsilon} R - \sqrt{\epsilon} R (\mathbb{1} + \epsilon Q) \right)}_{\epsilon^{3/2} [Q, R]} |00\rangle + \right. \\
& \quad \left. \underbrace{\left(\epsilon R^2 - \sqrt{\frac{\epsilon^2}{2}} \sqrt{2} R^2 \right)}_0 |10\rangle + \underbrace{\left(\epsilon R^2 - \sqrt{\frac{\epsilon^2}{2}} \sqrt{2} R^2 \right)}_0 |01\rangle + \mathcal{O}(\epsilon^2) \right] A_{n_{i+2}}^{[i+2]} \dots \quad (43)
\end{aligned}$$

Here $|n_i n_{i+1}\rangle \equiv |n_i\rangle \otimes |n_{i+1}\rangle$ are occupation number states. All terms of order ϵ inside the square brackets are seen to cancel, leaving a leading term $\propto \epsilon^{3/2}$ which cancels with the pre-factor $\frac{1}{\epsilon^{3/2}}$ to produce a finite result. Crucially, the cancellations of order ϵ involve basis states $|n_i = 2\rangle$ and $|n_{i+1} = 2\rangle$. A similar calculation for the case of $d = 2$ will result in a non-vanishing contribution of order ϵ , which will diverge in the limit $\epsilon \rightarrow 0$ (unless $R^2 = 0$). Thus, a Hilbert space dimension of $d = 2$ seems irreconcilable with a bosonic theory. However, if we modify the term $\frac{1}{\epsilon^{3/2}} (\mathbb{1}_i c_{i+1} - c_i \mathbb{1}_{i+1})$ to

$$\frac{1}{\epsilon^{3/2}} (\mathbb{1}_i c_{i+1} - c_i \mathbb{1}_{i+1}) \rightarrow \frac{1}{\epsilon^{3/2}} (\mathcal{P}_i^0 c_{i+1} - c_i \mathcal{P}_{i+1}^0), \quad (44)$$

with \mathcal{P}_i^0 a projection operator onto the empty state $|0\rangle$ at position x_i , it is easy to verify that all terms of order ϵ will vanish. Furthermore, the result of the operator application $\frac{1}{\epsilon^{3/2}} (\mathcal{P}_i^0 c_{i+1} - c_i \mathcal{P}_{i+1}^0) |\Psi\rangle$ is, to lowest order in ϵ , seen to be identical to Eq.(43). Similarly, the operator $c_i c_i$ in the interaction is not compatible with a local Hilbert space dimension of $d = 2$. To overcome this problem, we make the replacement

$$c_i c_i \rightarrow c_i c_{i+1}. \quad (45)$$

Similar to the kinetic energy operator, the result of $c_i c_{i+1} |\Psi\rangle$ is, to lowest order in ϵ , seen to be identical to that of $c_i c_i |\Psi\rangle$. After these replacements the final lattice Hamiltonian H assumes the form

$$\begin{aligned}
H(\epsilon) \equiv & -\frac{1}{2m\epsilon^2} \sum_i \left(c_i^\dagger c_{i+1} + h.c. \right) \\
& + \frac{1}{2m\epsilon^2} \sum_i \left(\mathcal{P}_i^0 c_{i+1}^\dagger c_{i+1} + c_i^\dagger c_i \mathcal{P}_{i+1}^0 \right) \\
& + \sum_i \mu_i c_i^\dagger c_i \\
& + \frac{g}{\epsilon} \sum_i c_i^\dagger c_{i+1}^\dagger c_i c_{i+1}. \quad , \quad (46)
\end{aligned}$$

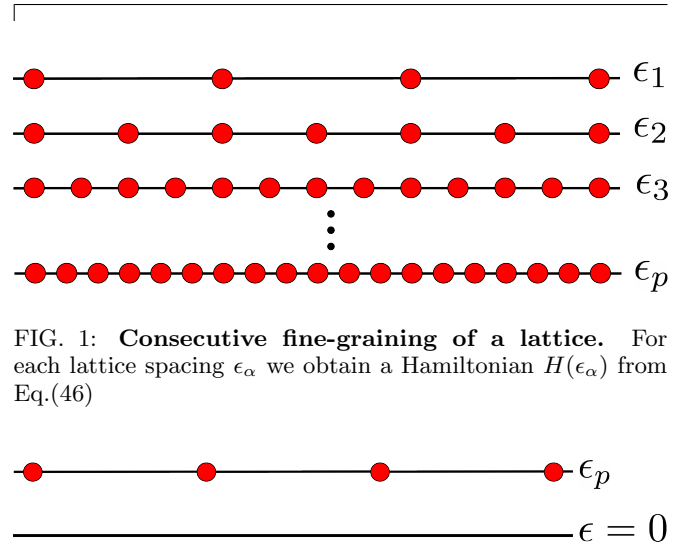


FIG. 1: **Consecutive fine-graining of a lattice.** For each lattice spacing ϵ_α we obtain a Hamiltonian $H(\epsilon_\alpha)$ from Eq.(46)

FIG. 2: **Obtaining a cMPS from a lattice MPS.** We extract the cMPS matrices $\{Q(x_i), R(x_i)\}$ from the ground-state $|\Psi(\epsilon_p)\rangle$ of a lattice optimization and use interpolation techniques to obtain continuous matrices $Q(x), R(x)$ (see Sec.III A).

and the MPS tensors are given by

$$\begin{aligned}
A_0^{[i]}(\epsilon) &= \mathbb{1} + \epsilon Q \\
A_1^{[i]}(\epsilon) &= \sqrt{\epsilon} R.
\end{aligned} \quad (47)$$

IV. A HYBRID MPS/CMPS ALGORITHM

In this section we describe an algorithm that takes a continuous, inhomogeneous Hamiltonian H of a non-relativistic QFT, and produces a cMPS approximation for its ground-state.

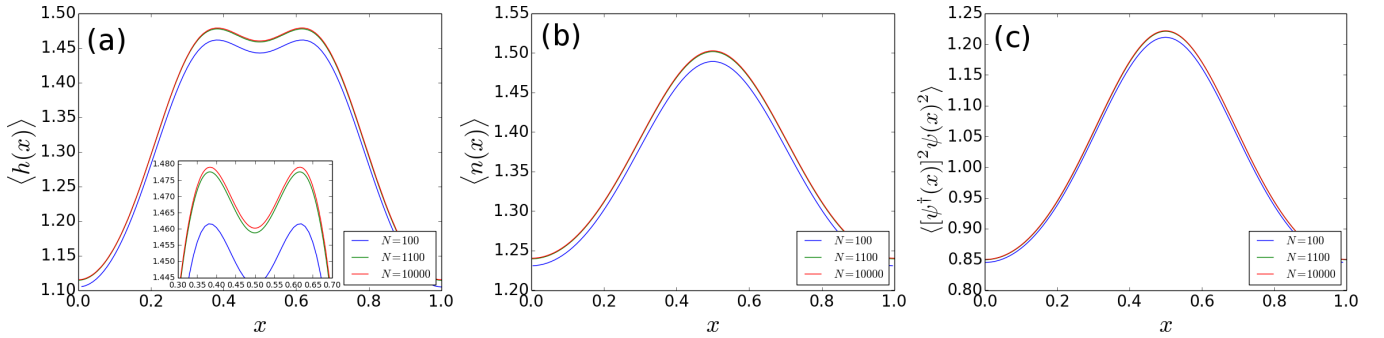


FIG. 3: **Ground-state observables for different lattices.** (a) Energy density $\langle h(x) \rangle \equiv \langle \frac{1}{2m} \partial_x \psi^\dagger(x) \partial_x \psi(x) + g \psi^\dagger(x) \psi^\dagger(x) \psi(x) \psi(x) \rangle$ of the ground-state of Eq.(1) for $D = 16, \mu_0 = -0.5, V_0 = -1.0, g = 1.0$, for different number of lattice points per unit-cell. (b) Particle density $\langle n(x) \rangle$ and (c) interaction term $\langle [\psi^\dagger(x)]^2 \psi^2(x) \rangle$ for the same ground-states as in (a).

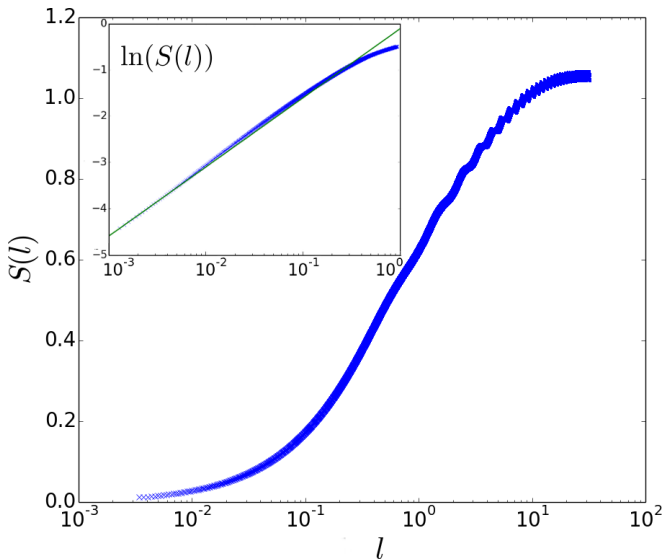


FIG. 4: **Entanglement entropy of a bulk region of length l .** Main figure: entanglement entropy $S(l)$ in the ground-state of Eq.(46) of a small region of length l as a function of l , for $D = 16, \mu_0 = -0.5, V_0 = -1.0, g = 1.0, L = 1.0$, and $N = 10^4$ lattice points per unit-cell. Oscillations are due to the periodicity of the state. Inset: $\ln(S(l))$ vs. $\log(l)$. For the smallest l visible, we see a power law increase in $S(l)$ which levels off for larger $l > 10^{-1}$. The point where the curvature in the figure changes sign is approximately at $l \approx 0.05$. The green line is a fit to the first 15 data-points.

A. Sequence of lattice Hamiltonians

To obtain a cMPS approximation $|\Psi\rangle$ for the ground-state of the continuum Hamiltonian H , we first construct a sequence of lattice Hamiltonians $H(\epsilon_\alpha), \alpha = 1 \dots p$, with $\epsilon_1 > \epsilon_2 \dots > \epsilon_p$. This is schematically represented in Fig. 1. We then sequentially compute a MPS approximation $|\Psi(\epsilon_\alpha)\rangle$ to the ground-state of Hamiltonian $H(\epsilon_\alpha)$. We initialize the ground-state optimization of $H(\epsilon_\alpha)$ using the extension of $|\Psi(\epsilon_{\alpha-1})\rangle$ to the lattice

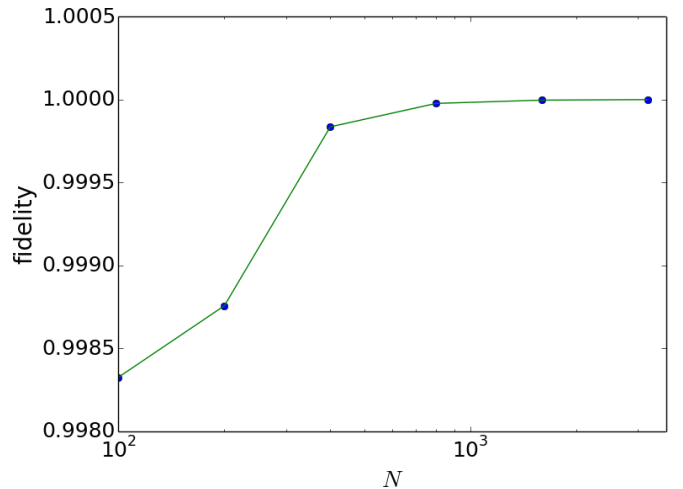


FIG. 5: **Quality of interpolation.** Fidelity per unit-cell of ground-states on $N = 100, 200, 400, 800, 1600$ and 3200 grid points per unit-cell after interpolation to $N_{final} = 3200$ with ground-state at $N_{final} = 3200$. Parameters are the same as in Fig. 3. Lines are guides to the eye.

$\mathcal{L}(\epsilon_\alpha)$, as described above. $|\Psi(\epsilon_1)\rangle$ is initialized with random, constant matrices Q, R . From the converged state $|\Psi(\epsilon_p)\rangle$ we then construct a cMPS approximation $|\Psi\rangle$ to the ground-state of the continuum Hamiltonian H , see Fig. 2.

B. Optimization of MPS with a finite unit-cell

For each Hamiltonian $H(\epsilon_\alpha)$ we obtain the ground-state from an infinite DMRG (iDMRG) method, as introduced by McCulloch^{4,44}, extended to the case of a large unit-cell with $N \gg 2$ sites. In Appendix D we present in detail the implementation for the cases considered in this manuscript, and explain possible variants of the algorithm, including a gradient-based optimization method for translation invariant lattices. Once the ground-state $|\Psi(\epsilon_\alpha)\rangle$ of $H(\epsilon_\alpha)$ has been found, we extract

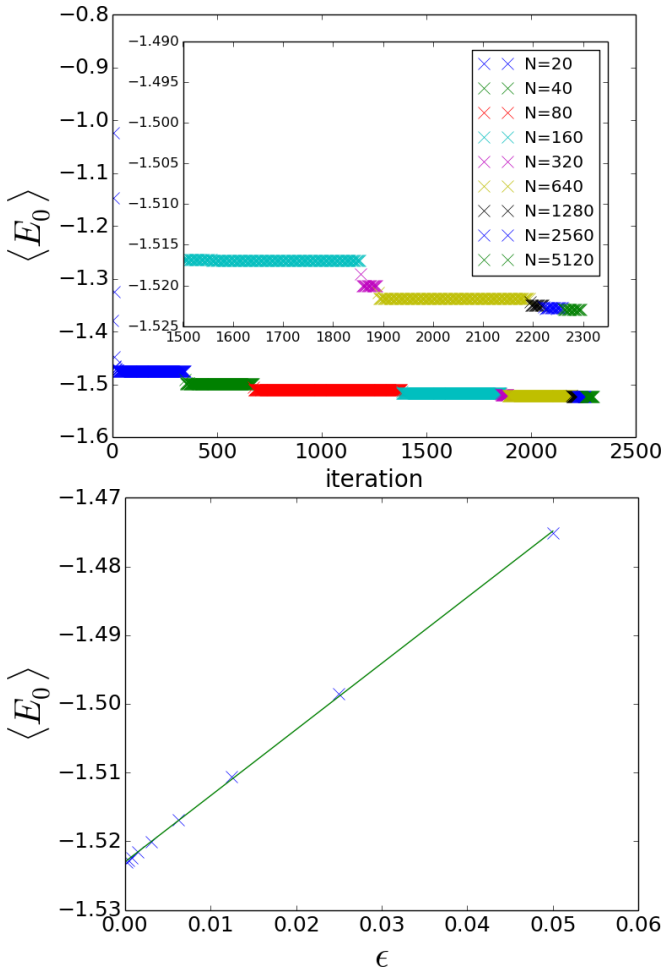


FIG. 6: **Convergence of the ground-state energy.** Upper panel: ground-state energy per unit-cell, as a function of DMRG sweeps for $\mu_0 = -0.5, V_0 = -1.0, g = 1.0, D = 32, L = 1.0$. The different colours correspond to different fine-graining. At each lattice spacing, ground-state energies are converged to 10^{-8} . Blue crosses at small iteration numbers are for $N = 20$ lattice sites; following crosses are obtained by taking the MPS from the previous discretization and using a spline interpolation on the matrices $Q(x_i), R(x_i)$ to obtain a finer discretization, and continue optimization for the fine-grained lattice. Lower panel: converged ground-state energy per unit-cell for different grid spacings ϵ .

the cMPS matrices $\{Q(x_i), R(x_i)\}$ and interpolate them to obtain an initial state $|\Psi'(\epsilon_{\alpha+1})\rangle$ for the optimization of the next Hamiltonian $H(\epsilon_{\alpha+1})$ (see Secs. III A and III B). Finally, after having obtained the ground-state $|\Psi(\epsilon_p)\rangle$ of $H(\epsilon_p)$, we use an interpolation to extract a cMPS approximation $Q(x), R(x)$ to the continuous ground-state, see Sec. III A.

V. EXAMPLE

In this section we present results for ground-states observables of Eq.(46) with a periodic background potential

Eq.(3) with periodicity $L = 1$. In particular, we show results for lattices $\mathcal{L}(\epsilon = \frac{L}{N})$ with an increasing number N of discretization points per unit-cell. For all calculations, we set $m = 0.5, g = 1.0, \mu_0 = -0.5$ and $V_0 = -1.0$. On each grid $\mathcal{L}(\frac{L}{N})$ we run the optimization until the energy per unit-cell is converged to 10^{-8} . In Fig. 3 (a), (b) and (c) we compare converged energy densities $\langle h(x) \rangle \equiv \langle \frac{1}{2m} \partial_x \psi^\dagger(x) \partial_x \psi(x) + g \psi^\dagger(x) \psi^\dagger(x) \psi(x) \psi(x) \rangle$, particle densities $\langle n(x) \rangle$ and interaction term $\langle [\psi^\dagger(x)]^2 \psi^2(x) \rangle$ from optimization on three different grids $N = 100$ (blue line), $N = 1100$ (green line) and $N = 10000$ (red line), obtained by successive interpolation from $N = 100$ to $N = 1100$, and from $N = 1100$ to $N = 10000$. We observe a clear convergence with increasing number of discretization points (the inset in Fig. 3 (a) zooms into the central region of the figure).

For large lattice spacing $\epsilon \geq 0.05$, we find that the interpolation method tends to perform worse than for small ϵ . Qualitatively, this follows from a dependence of the lattice matrices $Q(x_i, \epsilon), R(x_i, \epsilon)$ on the discretization ϵ . For large $\epsilon \geq 0.05$, we find that an interpolation to e.g. $\epsilon' = \epsilon/2$ and successive normalization of the MPS introduces changes in $Q(x_i, \epsilon), R(x_i, \epsilon)$ which are comparable to $Q(x_i, \epsilon), R(x_i, \epsilon)$. Thus, interpolation changes drastically the state. However, once the discretization is fine enough such that ϵ is well below a transition scale ξ (see below), corrections to $Q(x_i, \epsilon), R(x_i, \epsilon)$ from interpolation become much smaller than $Q(x_i, \epsilon), R(x_i, \epsilon)$, and interpolation in this case gives accurate ansatz states for finer grids. This can quantitatively be seen from analyzing for example the behaviour of the entanglement entropy $S(l) = -\text{tr}(\rho(l) \log(\rho(l)))$ of a bulk region of length l , where $\rho(l)$ is the reduced density matrix of this region. In Fig. 4 we show $S(l)$ for a ground-state on a very fine grid with $N = 10^4$ discretization points. Oscillations are due to the periodicity of the state. The inset shows $S(l)$ on a log-log scale. $S(l)$ exhibits a transition from a power law increase for $l < 0.05$ to a weaker increase for $l > 0.05$. This transition length scale $\xi \approx 0.05$ coincides with the region of the breakdown of the interpolation method, and depends on the location of the region l within the unit-cell (see Appendix C). The presence of a space dependent effective cutoff $\xi = \xi(x)$ suggests that it can be used to create optimal discretization grids for MPS by adjusting the grid distances $\epsilon(x)$ to $\xi(x)$. Note that this effective cutoff can be similarly seen in other physical observables like e.g. the superconducting correlation function $\langle \psi^\dagger(l) \psi(0) \rangle$ (not shown).

An appealing feature of the presented method is the fact that it gives access to a parametrization of the ground-state of an interacting quantum field theory in terms of a set of smooth functions $Q(x)$ and $R(x)$. This opens up new possible applications of lattice MPS methods. As described above, one application is the extension by interpolation of the ground state at one discretization to a new state at an arbitrarily finer discretization. Even though in general this new state will not be the ground-state of the finer lattice, it will be a good ap-

proximation to it, which can be used to initialize an optimization on the finer lattice. In particular, interpolation becomes an increasingly soft perturbation as one fine-grains the lattice. This is illustrated in Fig. 5, where we plot the fidelity per unit-cell of states obtained by interpolating the ground-states $|\Psi(\epsilon_\alpha)\rangle$ of lattices $\mathcal{L}(\epsilon_\alpha)$ with $N_\alpha = \{100, 200, 400, 800, 1600\}$, $\epsilon_\alpha = \frac{L}{N_\alpha}$ to a very fine lattice $\mathcal{L}(\epsilon_{final})$ with $N_{final} = 3200$, $\epsilon_{final} = \frac{L}{N_{final}}$. Each ground-state $|\Psi(\epsilon_\alpha)\rangle$ is obtained using a standard iDMRG optimization, and then extended to a state $|\Psi'_\alpha(\epsilon_{final})\rangle$ on $\mathcal{L}(\epsilon_{final})$. We then calculate the fidelity per unit-cell of the overlap $\langle \Psi'_\alpha(\epsilon_{final}) | \Psi(\epsilon_{final}) \rangle$. As can be seen from the figure, the fidelity rapidly converges towards 1.0, indicating that the interpolated, non-optimized state $|\Psi'_\alpha(\epsilon_{final})\rangle$ is very close to the true ground-state of the final lattice (see also Appendix B for further discussion on interpolation).

As we argue above, the speed of convergence of an optimization on a given lattice $\mathcal{L}(\epsilon')$ can be drastically improved by a proper choice of initialization. To this end, we use the proposed interpolation method to extend the MPS $|\Psi(\epsilon)\rangle$ from a previous optimization to the current lattice $\mathcal{L}(\epsilon')$. The resulting state $|\Psi'(\epsilon')\rangle$ is then used as initial state to the optimization on $\mathcal{L}(\epsilon')$. The merit of this approach is demonstrated in the upper panel of Fig. 6, where we show the ground-state energy per unit-cell as a function of the iteration number in the optimization (each iteration corresponds to a DMRG sweep over the unit-cell). After the energy is converged within 10^{-8} we take the state, prolong it to a finer grid and continue optimization. Different colors in the figure correspond to different number of lattice sites N per unit-cell. The inset zooms onto the right part of the figure. The lower panel in Fig. 6 shows the ground-state energy per unit-cell as a function of discretization parameter ϵ , with a clear linear behaviour in ϵ .

VI. DISCUSSION

As we have already mentioned in the introduction, our proposed method shares important similarities with the multigrid DMRG method proposed by Dolfi et al.³⁵. In this section we give a quantitative comparison between the multigrid approach and our proposed interpolation method. We start with a quick summary of the multigrid approach.

To transform an MPS from a lattice with N sites to a lattice with $N' = KN$ sites, with $K \in \mathbb{N}$, the multigrid approach splits up each tensor $A_{\tilde{n}_i}^{[i]}$ into a product of K new tensors $\tilde{A}_{\tilde{n}_1}^{[i_1]} \dots \tilde{A}_{\tilde{n}_K}^{[i_K]}$. The splitting is performed by first contracting $A_{\tilde{n}_i}^{[i]}$ with a tensors $T_{\tilde{n}_1, \dots, \tilde{n}_K}^{n_i}$,

$$T_{\tilde{n}_1, \dots, \tilde{n}_K}^{n_i} = \frac{\delta(n_i, \sum_{\alpha=1}^K \tilde{n}_\alpha)}{\sqrt{\sum_{n'_1, \dots, n'_K} \delta(n_i, \sum_{\alpha=1}^K n'_\alpha)}}, \quad (48)$$

and then using an SVD to decompose the resulting tensor

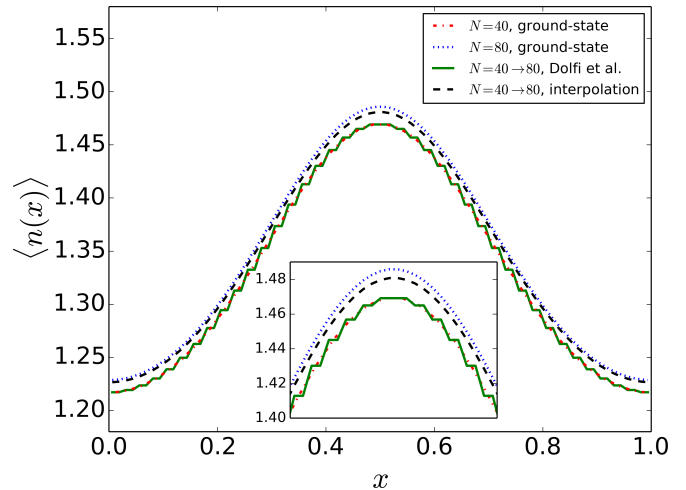


FIG. 7: **Particle density $\langle n(x) \rangle$ for different interpolation schemes.** Starting from the ground-state of lattice with $N = 40$ per unit-cell (red dash-dotted line), we use prolongation as proposed by Dolfi et al. (green solid line) and our proposed interpolation method (black dashed line) to obtain a state on a finer lattice with $N = 80$ sites per unit-cell. For comparison we also show $\langle n(x) \rangle$ for the optimized ground-state on $N = 80$ sites per unit-cell. The inset shows a magnification of the central peak.

into a product of K tensors $\tilde{A}_{\tilde{n}_1}^{[i_1]} \dots \tilde{A}_{\tilde{n}_K}^{[i_K]}$. For the case of $K = 2$, this is graphically represented as

(49)

(see the Appendix for a short summary of diagrammatic MPS notations). Note that the bond dimension between the two new tensors has increased, which we have indicated by drawing a thicker line between the two.

To compare the multigrid approach with our interpolation method, we start from a ground-state on a lattice with $N = 40$ sites per unit-cell, and extend this state to a grid with $N = 80$ sites per unit-cell, using the multigrid approach and our proposed interpolation method. In Fig. 7 we show results for the particle density $\langle n(x_i) \rangle$ for the different approaches. The red dash-dotted line shows $\langle n(x_i) \rangle$ for the ground-state on $N = 40$ lattice sites per unit-cell. The green solid and black dashed line are the results from the extension to a lattice with $N = 80$ sites using a multigrid approach and our interpolation method, respectively. The blue dotted line is the ground-state for the $N = 80$ site lattice. From this result we see that the multigrid approach already gives a good ansatz state. However, the prolongation here produces step-like artifacts. The interpolation on the other hand produces a smooth density profile which is seen to be already very close to the true ground-state density profile on a lattice with $N = 80$ sites per unit-cell. The inset shows a zoom onto the central region. Note that the total particle

number is not fixed in our model.

VII. CONCLUSION

We have presented a method which unifies the continuous matrix product state representation for quantum fields with standard optimization techniques for MPS on the lattice. Our method is equally applicable to both translation invariant and inhomogeneous systems, as we demonstrate for an interacting bosonic field in a periodic potential. Starting from a continuum Hamiltonian H , we construct a sequence of discretized Hamiltonians $\{H(\epsilon_\alpha)\}_{\alpha=1,2,\dots,p}$ on increasingly finer lattices $\mathcal{L}(\epsilon_\alpha)$ with lattice spacings $\epsilon_1 > \epsilon_2 > \dots > \epsilon_p$. Our method is initialized by using energy minimization for lattice MPS to optimize an MPS approximation $|\Psi(\epsilon_1)\rangle$ to the ground-state of $H(\epsilon_1)$. We then use the MPS $|\Psi(\epsilon_\alpha)\rangle$ optimized for the ground state of $H(\epsilon_\alpha)$ to initialize the energy minimization for Hamiltonian $H(\epsilon_{\alpha+1})$, resulting in the optimized MPS $|\Psi(\epsilon_{\alpha+1})\rangle$. To initialize the optimization we make use of the hidden cMPS structure of the MPS $|\Psi(\epsilon_\alpha)\rangle$ to extend it from the lattice $\mathcal{L}(\epsilon_\alpha)$ to the lattice $\mathcal{L}(\epsilon_{\alpha+1})$. From the final MPS $|\Psi(\epsilon_p)\rangle$ for the ground state of $H(\epsilon_p)$, we then extract the cMPS approximation $|\Psi\rangle$ for the ground state of H directly in

the continuum. For the variational energy optimization, we introduce a new procedure to discretize H into a lattice model where each site contains a two-dimensional vector space (spanned by vacuum $|0\rangle$ and one boson $|1\rangle$ states). Our method can be generalized to the case of multiple species of bosons or fermions, or even mixtures of both.

Acknowledgements

The authors thank J. Rincón, F. Verstraete and D. Draxler for insightful discussions. The authors also acknowledge support by the Simons Foundation (Many Electron Collaboration). Computations were made on the supercomputer Mammouth parallèle II from University of Sherbrooke, managed by Calcul Québec and Compute Canada. The operation of this supercomputer is funded by the Canada Foundation for Innovation (CFI), the ministère de l'Économie, de la science et de l'innovation du Québec (MESI) and the Fonds de recherche du Québec - Nature et technologies (FRQ-NT). This research was supported in part by Perimeter Institute for Theoretical Physics. Research at Perimeter Institute is supported by the Government of Canada through Industry Canada and by the Province of Ontario through the Ministry of Economic Development & Innovation.

* corresponding author: martin.ganahl@gmail.com

¹ M. Fannes, B. Nachtergaele, and R. F. Werner, *Communications in Mathematical Physics* **144**, 443 (1992).
² U. Schollwöck, *Annals of Physics* **326**, 96 (2011).
³ F. Verstraete, J. I. Cirac, and V. Murg, arXiv:0907.2796 (2009).
⁴ S. R. White, *Physical Review Letters* **69**, 2863 (1992).
⁵ G. Vidal, *Physical Review Letters* **99**, 220405 (2007).
⁶ F. Verstraete and J. I. Cirac, arXiv:cond-mat/0407066 (2004).
⁷ E. M. Stoudenmire, L. O. Wagner, S. R. White, and K. Burke, *Physical Review Letters* **109**, 056402 (2012).
⁸ A. Milsted, J. Haegeman, and T. J. Osborne, *Physical Review D* **88**, 085030 (2013).
⁹ L. O. Wagner, E. M. Stoudenmire, K. Burke, and S. R. White, *Physical Review Letters* **111** (2013).
¹⁰ L. O. Wagner, T. E. Baker, E. M. Stoudenmire, K. Burke, and S. R. White, *Physical Review B* **90**, 045109 (2014).
¹¹ T. E. Baker, E. M. Stoudenmire, L. O. Wagner, K. Burke, and S. R. White, *Physical Review B* **91**, 235141 (2015).
¹² T. E. Baker, E. M. Stoudenmire, L. O. Wagner, K. Burke, and S. R. White, *Physical Review B* **93**, 119912(E) (2016).
¹³ E. M. Stoudenmire and S. R. White, *Physical Review Letters* **119**, 046401 (2017).
¹⁴ T. E. Baker, K. Burke, and S. R. White, arXiv:1709.03460 [physics] (2017).
¹⁵ F. Verstraete and J. I. Cirac, *Physical Review Letters* **104**, 190405 (2010).
¹⁶ J. Haegeman, J. I. Cirac, T. J. Osborne, H. Verschelde, and F. Verstraete, *Physical Review Letters* **105**, 251601 (2010).

¹⁷ J. Haegeman, T. J. Osborne, H. Verschelde, and F. Verstraete, *Physical Review Letters* **110**, 100402 (2013).
¹⁸ M. Miyaji, T. Numasawa, N. Shiba, T. Takayanagi, and K. Watanabe, *Physical Review Letters* **115**, 171602 (2015).
¹⁹ Q. Hu and G. Vidal, *Physical Review Letters* **119**, 010603 (2017).
²⁰ A. Franco-Rubio and G. Vidal, arXiv:1706.02841 [cond-mat, physics:hep-th, physics:quant-ph] (2017).
²¹ X. Wen, G. Y. Cho, P. L. S. Lopes, Y. Gu, X.-L. Qi, and S. Ryu, *Physical Review B* **94**, 075124 (2016).
²² J. Molina-Vilaplana, *Journal of High Energy Physics* **2015**, 2 (2015).
²³ J. S. Cotler, J. Molina-Vilaplana, and M. T. Mueller, arXiv:1612.02427 [hep-th, physics:quant-ph] (2016).
²⁴ D. Draxler, J. Haegeman, T. J. Osborne, V. Stojevic, L. Vanderstraeten, and F. Verstraete, *Physical Review Letters* **111**, 020402 (2013).
²⁵ F. Quijandría, J. J. García-Ripoll, and D. Zueco, *Physical Review B* **90**, 235142 (2014).
²⁶ S. S. Chung, K. Sun, and C. J. Bolech, arXiv:1501.00228 [cond-mat, physics:quant-ph] (2014).
²⁷ F. Quijandría and D. Zueco, *Physical Review A* **92**, 043629 (2015).
²⁸ J. Haegeman, D. Draxler, V. Stojevic, J. I. Cirac, T. J. Osborne, and F. Verstraete, arXiv:1501.06575 [cond-mat, physics:hep-th, physics:math-ph, physics:nlin, physics:quant-ph] (2015).
²⁹ J. Rincón, M. Ganahl, and G. Vidal, *Physical Review B* **92**, 115107 (2015).
³⁰ S. S. Chung, K. Sun, and C. J. Bolech, *Physical Review B* **91**, 121108 (2015).

- ³¹ D. Draxler, J. Haegeman, F. Verstraete, and M. Rizzi, arXiv:1609.09704 [cond-mat, physics:quant-ph] (2016).
- ³² M. Ganahl, J. Rincón, and G. Vidal, Physical Review Letters **118**, 220402 (2017).
- ³³ M. Ganahl, arXiv:1712.01260 [cond-mat, physics:physics] (2017).
- ³⁴ J. Haegeman, J. I. Cirac, T. J. Osborne, I. Pižorn, H. Verschelde, and F. Verstraete, Physical Review Letters **107**, 070601 (2011).
- ³⁵ M. Dolfi, B. Bauer, M. Troyer, and Z. Ristivojevic, Physical Review Letters **109**, 020604 (2012).
- ³⁶ M. A. Cazalilla, Journal of Physics B: Atomic, Molecular and Optical Physics **37**, S1 (2004).
- ³⁷ E. H. Lieb and W. Liniger, Physical Review **130**, 1605 (1963).
- ³⁸ E. H. Lieb, Physical Review **130**, 1616 (1963).
- ³⁹ L. P. Pitaevskii, Journal of Experimental and Theoretical Physics **13**, 451 (1961).
- ⁴⁰ E. P. Gross, Il Nuovo Cimento (1955-1965) **20**, 454 (1961).
- ⁴¹ E. P. Gross, Journal of Mathematical Physics **4**, 195 (1963).
- ⁴² J. Haegeman, J. I. Cirac, T. J. Osborne, and F. Verstraete, Physical Review B **88**, 085118 (2013).
- ⁴³ H. Bachau, E. Cormier, P. Decleva, J. E. Hansen, and F. Martín, Reports on Progress in Physics **64**, 1815 (2001).
- ⁴⁴ I. P. McCulloch, 0804.2509 (2008).
- ⁴⁵ R. Ors and G. Vidal, Physical Review B **78**, 155117 (2008).
- ⁴⁶ E. M. Stoudenmire and S. R. White, Physical Review B **87**, 155137 (2013).
- ⁴⁷ V. Zauner-Stauber, L. Vanderstraeten, M. T. Fishman, F. Verstraete, and J. Haegeman, arXiv:1701.07035 [cond-mat, physics:quant-ph] (2017).

Appendix A: Shifting of the orthogonality center and gauging

In the following we describe how to shift the orthogonality center of an MPS. For the discrete lattice case presented in this manuscript, we use a QR decomposition on the tensors $A^{[i]}$ to shift the orthogonality center. However, to keep the cMPS form explicit, that is keep matrices in the form Eq.(47), we use an approach which is slightly different from the standard procedure. The generic form of an MPS after a local optimization step at site $i + 1$ is

$$\dots \left(\begin{array}{c} \mathbb{1} + \epsilon Q^l(x_i) \\ \sqrt{\epsilon} R^l(x_i) \end{array} \right) \left(\begin{array}{c} V(x_{i+1}) \\ \sqrt{\epsilon} R(x_{i+1}) \end{array} \right) \left(\begin{array}{c} \mathbb{1} + \epsilon Q^r(x_{i+2}) \\ \sqrt{\epsilon} R^r(x_{i+2}) \end{array} \right) \dots$$

where superscripts l/r indicate left or right orthonormal matrices^{33,42}. Pulling out $V(x_{i+1})$ yields

$$\dots \left(\begin{array}{c} \mathbb{1} + \epsilon Q^l(x_i) \\ \sqrt{\epsilon} R^l(x_i) \end{array} \right) \left(\begin{array}{c} \mathbb{1} \\ \sqrt{\epsilon} R(x_{i+1}) [V(x_{i+1})]^{-1} \end{array} \right) V(x_{i+1}) \\ \times \left(\begin{array}{c} \mathbb{1} + \epsilon Q^r(x_{i+2}) \\ \sqrt{\epsilon} R^r(x_{i+2}) \end{array} \right) \dots$$

Using a QR decomposition, the center term in brackets is then orthonormalized:

$$\left(\begin{array}{c} \mathbb{1} \\ \sqrt{\epsilon} R(x_{i+1}) [V(x_{i+1})]^{-1} \end{array} \right) \xrightarrow{QR} \left(\begin{array}{c} \mathbb{1} + \epsilon Q^l(x_{i+1}) \\ \sqrt{\epsilon} R^l(x_{i+1}) \end{array} \right) C(x_{i+1}).$$

The matrix product $C(x_{i+1})V(x_{i+1})$ is then normalized and absorbed into the matrices at site $i + 2$. A similar procedure is applied to shift the center site to the left. Crucially, we find that the standard QR algorithm in *numpy*, equipped with a phase-convention for the diagonal of R (not be confused with the cMPS matrix), preserves the cMPS form of the tensors. Note that due to the gauge freedom of (c)MPS, the matrices $R(x_i)$ and $Q(x_i)$ do not need to be continuous, even in the limit $\epsilon \rightarrow 0$. For a random initial state, we observe that during the local updates, matrices $Q(x_i)$ and $R(x_i)$ develop discontinuities. These jumps, however, become smaller and eventually disappear as one approaches convergence, resulting in smooth matrix functions $R(x_i), Q(x_i)$ within the unit-cell.

However, the orthonormalization procedure described above introduces a non-trivial gauge change as one moves from one side of the unit-cell to the other. As a result, the matrices $Q(x_i), R(x_i)$ do not trivially connect back to themselves at the end of the unit-cell, even if they originally did. For the purpose of interpolating the matrices a smooth gauge is favourable. To this end, we first canonize the unit-cell MPS by calculating the left and right eigen-vectors l and r of the unit-cell transfer operator

$$T_{UC} = \sum_{\{n_i\}} (A_{n_1}^{[1]} \dots A_{n_N}^{[N]}) \otimes (\bar{A}_{n_1}^{[1]} \dots \bar{A}_{n_N}^{[N]}), \quad (\text{A1})$$

from which we obtain $X \equiv \sqrt{r}$ and $Y \equiv \sqrt{l}$. We then compute $U\lambda V = YX$, and absorb $V^\dagger X^{-1}$ into the leftmost and $Y^{-1}U\lambda$ into the rightmost MPS matrix. Sweeping from right to left, we then successively orthonormalize the matrices using an SVD on the matrices $A_{n_i}^{[i]} = U^{[i]} \lambda^{[i]} V_{n_i}^{[i]}$ (indices $[i]$ in square brackets are position labels). To fix the gauge freedom of the SVD, we fix the diagonal of the right isometry $V_{n_i}^{[i]}$ to be real and positive. In a successive sweep from the left to the right boundary we fix the diagonal of the matrix $U_{n_i}^{[i]}$ in $A_{n_i}^{[i]} = U_{n_i}^{[i]} \lambda^{[i]} V^{[i]}$ to be real and positive. The right boundary matrix $V^{[N]}$ will then be a diagonal unitary matrix which can be distributed over the unit-cell:

$$e^{i\mathcal{H}L} \equiv V^{[N]} = \prod_i^N e^{i\epsilon\mathcal{H}} \equiv \prod_i^N G \quad (\text{A2})$$

where L is the length of the unit-cell, N is the number of lattice points, $\epsilon = L/N$, and \mathcal{H} is a hermitian operator. G is close to the identity and can be written as $G = \mathbb{1} + \epsilon\tilde{\mathcal{H}}$, with $\tilde{\mathcal{H}}$ an almost hermitian operator. $V^{[N]}$ can now be equally distributed over all matrices by the following two steps: First, at every site $i \in \{1 \dots N\}$ transform the matrices $Q(x_i), R(x_i)$ according to

$$\begin{aligned} Q(x_i) &\leftarrow (G^\dagger)^{i-1} Q(x_i) G^{i-1} \\ R(x_i) &\leftarrow (G^\dagger)^{i-1} R(x_i) G^{i-1}. \end{aligned} \quad (\text{A3})$$

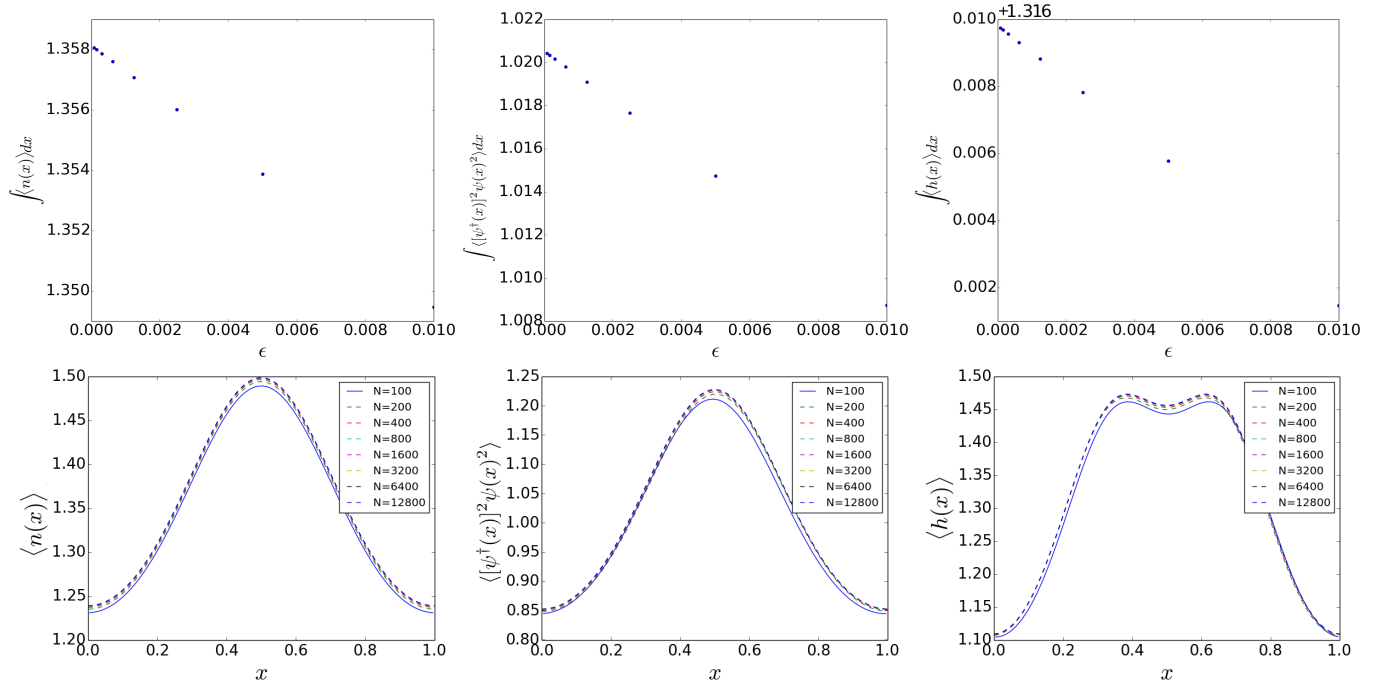


FIG. A1: **Convergence of interpolation scheme for different final grid-spacings.** We start with a ground-state on a grid of $N = 100$ sites per unit-cell and interpolate it, using spline interpolation, to different final grids (see legend). The upper panel (from left to right) shows the total particle number $\int_0^L \langle n(x) \rangle dx$, the total interaction energy $\int_0^L \langle [\psi^\dagger(x)]^2 \psi^2(x) \rangle dx$ and total energy $\int_0^L \langle h(x) \rangle dx$ (see main text) as a function of grid spacing ϵ . Each shows linear dependence on ϵ . Lower panel: spatially resolved $\langle n(x) \rangle$, $\langle [\psi^\dagger(x)]^2 \psi^2(x) \rangle$ and $\langle h(x) \rangle$ for different number N of final lattice points per unit-cell.

Second, transform each matrix

$$\begin{aligned} Q(x_i) &\leftarrow Q(x_i) + \tilde{\mathcal{H}} + \epsilon Q(x_i) \tilde{\mathcal{H}} \\ R(x_i) &\leftarrow R(x_i) + \epsilon R(x_i) \tilde{\mathcal{H}} \end{aligned} \quad (\text{A4})$$

The resulting matrices $Q(x_i), R(x_i)$ will connect smoothly back to themselves.

Appendix B: Continuous limit of fine-graining

In this section we explore in more detail how interpolation affects different observables. In particular, we will focus on the observables $\langle n(x) \rangle$, $\langle [\psi^\dagger(x)]^2 \psi^2(x) \rangle$ and $\langle h(x) \rangle$ (see also main text). We first obtain the ground-state of Eq.(46) for $D = 16, \mu_0 = -0.5, V_0 = -1.0, g = 1.0$ and $N = 100$ sites per unit-cell. We then interpolate the corresponding matrices $Q(x_i), R(x_i)$ to different finer grids with $N = 200, 400, 800, 1600, 3200, 6400$ and 12800 sites per unit-cell, and calculate the observables $\langle n(x) \rangle$, $\langle [\psi^\dagger(x)]^2 \psi^2(x) \rangle$ and $\langle h(x) \rangle$ after normalizing the state. The results are shown in Fig. A1. The upper panel shows $\int_0^L dx \langle n(x) \rangle$, $\int_0^L dx \langle [\psi^\dagger(x)]^2 \psi^2(x) \rangle$ and $\int_0^L dx \langle h(x) \rangle$, integrated over the unit-cell, as a function of ϵ . We observe a clear linear dependence on ϵ as we decrease the lattice spacing. The lower panel shows the spatially resolved quantities for different N .

Appendix C: Short range entanglement

In Fig. 4 in the main text we show how the entanglement entropy $S(l)$ of a region of size l in the center of the unit-cell (for parameters $D = 16, \mu_0 = -0.5, V_0 = -1.0, g = 1.0$, see Fig. 3). As pointed out in the main text we observe a transition from a power law increase for small l to a less pronounced increase for larger l at a certain length scale $\xi \approx 0.05$. Fig. A2 shows $S(l)$ for two different locations of the region l , namely in the center of the unit-cell and close to the left boundary of the unit-cell (with l growing to the right). The plot illustrates that ξ varies along the unit-cell, which could be used as basis for determining grid spacings for non-homogeneous discretizations as e.g. shown in Fig. 1 in the main text.

Appendix D: Optimization of periodic MPS on a lattice

In this section we give a detailed description of the optimization method used to obtain the ground-state of a Hamiltonian $H(\epsilon_\alpha)$ (see main text). We employ the infinite DMRG (iDMRG) method as introduced by McCulloch⁴⁴, extended to the case of a large unit-cell with $N \gg 2$ sites. To make the document self-contained, we give in the following a detailed explanation of the al-

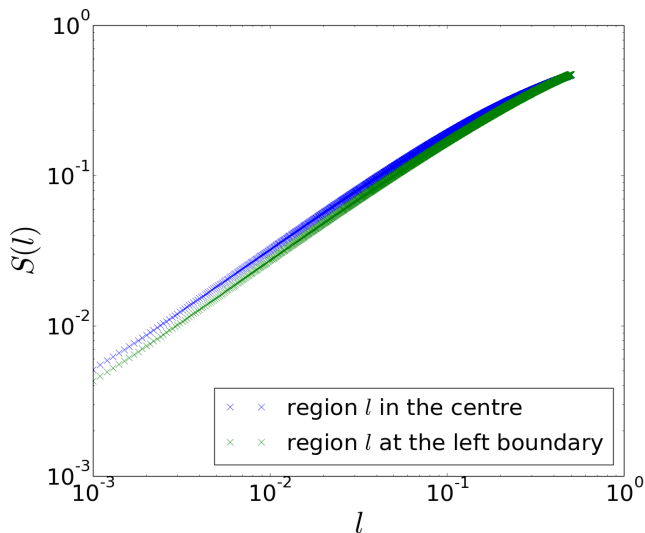


FIG. A2: **Entanglement entropy $S(l)$ as a function of length l .** Entanglement entropy $S(l)$ of region of length l in the ground-state of Eq.(46) for $D = 16, \mu_0 = -0.5, V_0 = -1.0, g = 1.0, L = 1.0$, and $N = 10^4$ lattice points per unit-cell. We show $S(l)$ for two different regions l : blue crosses show $S(l)$ as a function of l for l starting at the center of the unit-cell, and green crosses show $S(l)$ for l starting close to the left boundary. For the latter case we see that $S(l)$ departs from the linear behaviour at a larger length scale than for l in the center of the unit-cell. This fact could be used devise non-homogeneous discretization schemes for MPS that use a varying grid spacing based on this length scale. Note that the slope of both curves is very similar, which could suggest a universal short lengths scale behaviour of the entanglement entropy.

gorithm. For the sake of simplicity, we restrict ourselves to the case of $N = 4$. Results for arbitrary N follow straightforwardly.

Before going into more detail, we first introduce some necessary diagrammatic notations for MPS. In the following we consider periodic MPS with N tensors $\{A^{[1]}, \dots, A^{[N]}\}$ per unit-cell. Such a state is pictorially represented as

$$|\Psi\rangle = \dots \left[\underset{j}{1} \right] \left[\underset{j}{2} \right] \left[\underset{j}{3} \right] \left[\underset{j}{4} \right] \dots, \quad (\text{D1})$$

where dots indicate an infinite repetition of the unit-cell. Subscripts $j \in \mathbb{Z}$ label the unit-cell. For brevity, we will in the following omit dots and subscripts j if no confusion can arise. Using standard regauging techniques⁴⁵ (see Appendix A), the state can be regauged into left and right orthogonal forms

$$|\Psi\rangle = \left[\underset{i}{1} \right] \left[\underset{i}{2} \right] \left[\underset{i}{3} \right] \left[\underset{i}{4} \right] = \left[\underset{i}{1} \right] \left[\underset{i}{2} \right] \left[\underset{i}{3} \right] \left[\underset{i}{4} \right]. \quad (\text{D2})$$

The left and right orthogonal tensors $\left[\underset{i}{\leftarrow} \right]$ and $\left[\underset{i}{\rightarrow} \right]$ obey

$$\left[\underset{i}{\leftarrow} \right] \left[\underset{i}{\rightarrow} \right] = \left(\quad \right) \quad (\text{D3})$$

$$\left[\underset{i}{\rightarrow} \right] \left[\underset{i}{\leftarrow} \right] = \left) \quad (\text{D4})$$

(see also Eq.(30)).

Of particular use is the so-called canonical form⁴⁵ of an MPS, given by the following decomposition:

$$|\Psi\rangle = \left[\underset{i}{1} \right] \left[\underset{i}{1} \right] \left[\underset{i}{2} \right] \left[\underset{i}{2} \right] \left[\underset{i}{3} \right] \left[\underset{i}{3} \right] \left[\underset{i}{4} \right] \left[\underset{i}{4} \right]. \quad (\text{D5})$$

$\left[\underset{i}{\circ} \right]$ are diagonal bond matrices containing the Schmidt values λ_α on bond i , and $\Gamma_{\alpha\beta}^{n,[i]} \equiv \left[\underset{i}{\diamond} \right]$ is a $D \times D \times d$ tensor at site i . In our convention, the index label i of a bond matrix can be deduced from the index of the left tensor next to it. For the sake of brevity, we will thus omit it if no confusion can arise. We will use angle brackets to denote inverses of matrices, i.e. $\left[\underset{i}{\square} \right]$ is the inverse of $\left[\underset{i}{\circ} \right]$, with $\left[\underset{i}{\square} \right] \left[\underset{i}{\circ} \right] = \left[\underset{i}{\circ} \right] \left[\underset{i}{\square} \right] = \text{---} \equiv \mathbb{1}$. The canonical form is particularly useful because the left and right orthogonal form of the MPS can be easily extracted using the relations

$$\left[\underset{i}{\circ} \right] \left[\underset{i}{\diamond} \right] = \left[\underset{i}{\leftarrow} \right] \quad (\text{D6})$$

$$\left[\underset{i}{\diamond} \right] \left[\underset{i}{\circ} \right] = \left[\underset{i}{\rightarrow} \right]. \quad (\text{D7})$$

Finally, we introduce the parallel decomposition⁴⁶

$$|\Psi\rangle = \left[\underset{i}{\square} \right] \left[\underset{i}{1} \right] \left[\underset{i}{2} \right] \left[\underset{i}{\circ} \right] \left[\underset{i}{3} \right] \left[\underset{i}{4} \right] \left[\underset{i}{\square} \right] \left[\underset{i}{1} \right] \left[\underset{i}{2} \right] \left[\underset{i}{\circ} \right] \left[\underset{i}{3} \right] \left[\underset{i}{4} \right] \left[\underset{i}{\square} \right] \left[\underset{i}{1} \right] \left[\underset{i}{2} \right] \left[\underset{i}{\circ} \right] \left[\underset{i}{3} \right] \left[\underset{i}{4} \right] \left[\underset{i}{\square} \right], \quad (\text{D8})$$

obtained e.g. from the canonical form by inserting identities $\left[\underset{i}{\square} \right] \left[\underset{i}{\circ} \right]$ and using Eqs.(D6) and (D7). Each unit-cell is here decomposed into a set of left and right orthogonal tensors, with matrices $\left[\underset{i}{\circ} \right]$ and $\left[\underset{i}{\square} \right]$ between the connection points. The positions of the matrices $\left[\underset{i}{\circ} \right]$ in Eq.(D8) are called the orthogonality centers. The matrices $\left[\underset{i}{\circ} \right]$ can be shifted inside the unit-cell using a QR or SV decomposition,

$$\left[\underset{i}{\leftarrow} \right] \left[\underset{i}{\circ} \right] = \left[\underset{i-1}{\circ} \right] \left[\underset{i}{\leftarrow} \right] \quad (\text{D9})$$

In particular, they can be shifted to the unit-cell boundaries, where they can be absorbed into $\left[\underset{i}{\square} \right]$. A defining

property of the parallel decomposition is that this absorption results in $\begin{bmatrix} \bigcirc & \bigcirc \\ \bigcirc & \bigcirc \end{bmatrix} \begin{bmatrix} \bigcirc \\ \bigcirc \end{bmatrix} = U_l$ and $\begin{bmatrix} \bigcirc & \bigcirc \\ \bigcirc & \bigcirc \end{bmatrix} \begin{bmatrix} \bigcirc \\ \bigcirc \end{bmatrix} = U_r$, with *unitary* matrices U_l, U_r . This implies that within each unit-cell local truncation of the MPS bond-dimension can be done optimally. The parallel decomposition is also central to the parallel version of DMRG on finite lattices⁴⁶.

In the following we explain the different steps involved in the ground-state optimization of a periodic Hamiltonian H in the thermodynamic limit. At each step of the optimization, the state is represented by N unit-cell tensors $\{A^{[1]}, \dots, A^{[N]}\}$ which can be patched into an infinite MPS. Fig. A3 gives an overview of the first five steps of the algorithm. Different colours of matrices and tensors indicate an update. In Fig. A3 (a), the MPS is initialized with N random tensors per unit-cell and brought into the parallel decomposition (red tensors and matrices in Fig. A3 (a)). The initial matrices $\begin{bmatrix} \bigcirc \\ \bigcirc \end{bmatrix}$ are diagonal, containing the Schmidt values. The tensors of each unit-cell are then updated using standard variational optimization techniques for MPS (see below for details), see Fig. A3 (b). The updated objects are shown in green, and updates are identical between each unit-cell. Note that the matrices $\begin{bmatrix} \bigcirc \\ \bigcirc \end{bmatrix}$ are dense. Between each unit-cell resides a matrix $\begin{bmatrix} \bigcirc & \bigcirc \\ \bigcirc & \bigcirc \end{bmatrix}$ from the previous step. (c) A resolution of identity is inserted. Using the QR or SV decomposition, the two matrices $\begin{bmatrix} \bigcirc \\ \bigcirc \end{bmatrix}$ at the orthogonality centers are shifted left, respectively right (see Eq.(D9)), until the boundary matrix $\begin{bmatrix} \bigcirc & \bigcirc \\ \bigcirc & \bigcirc \end{bmatrix}$ is reached (Fig. A3 (d)). The three matrices $\begin{bmatrix} \bigcirc & \bigcirc \\ \bigcirc & \bigcirc \end{bmatrix}$ are contracted into a new matrix $\begin{bmatrix} \bigcirc \\ \bigcirc \end{bmatrix}$ (see Fig. A3 (a')). The state is now in what we call *quasi-parallel decomposition* with respect to a new unit-cell that has been shifted by $N/2$. Quasi-parallel refers to the fact that $\begin{bmatrix} \bigcirc & \bigcirc \\ \bigcirc & \bigcirc \end{bmatrix}$ and $\begin{bmatrix} \bigcirc & \bigcirc \\ \bigcirc & \bigcirc \end{bmatrix}$ are in general both non-unitary. Note that during the optimization, the matrices will converge to unitary matrices. The degree of unitarity of the matrices $\begin{bmatrix} \bigcirc & \bigcirc \\ \bigcirc & \bigcirc \end{bmatrix}$ and $\begin{bmatrix} \bigcirc & \bigcirc \\ \bigcirc & \bigcirc \end{bmatrix}$ can be used as an alternative measure of convergence. This completes the first iteration of the algorithm. In the next iteration, the tensors of the new unit-cell $\{N/2 + 1, \dots, N, 1 \dots N/2\}$ are then going to be updated. Over time, several slightly different variants of how to proceed at this point have been developed. We will below explain three different approaches, which we find the most convenient one for our case. Before, however, let us first explain in more detail the individual steps in Fig. A3.

We start with the update from (a) to (b). Within each unit-cell, we use standard variational MPS optimization^{2,4} for a finite system to update the tensors. For a given, fixed unit-cell, the updated tensors $\{\tilde{A}^{[1]}, \dots, \tilde{A}^{[N]}\}$ are found from minimizing the expectation value of the energy with respect to the unit-cell

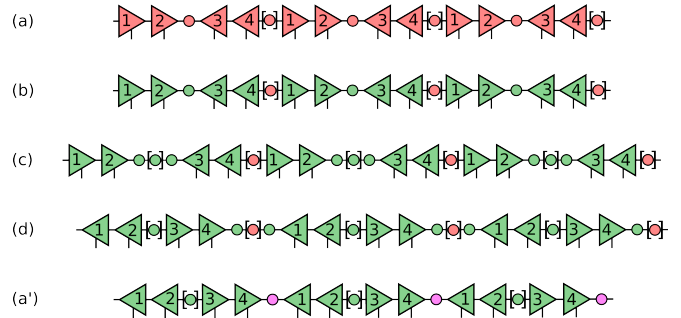


FIG. A3: **Outline of the first steps of an iDMRG calculation.** (a) Initial state in parallel decomposition. (b) State after all unit-cell tensors have been updated. (c) An identity resolution is inserted at the center of each unit-cell. (d) The tensors $\begin{bmatrix} \bigcirc \\ \bigcirc \end{bmatrix}$ are moved to the left respectively right unit-cell boundaries. (a') The two matrices $\begin{bmatrix} \bigcirc & \bigcirc \\ \bigcirc & \bigcirc \end{bmatrix}$ are contracted into $\begin{bmatrix} \bigcirc \\ \bigcirc \end{bmatrix}$.

tensors, i.e.

$$\{\tilde{A}^{[1]}, \dots, \tilde{A}^{[N]}\} = \underset{\{A^{[1]}, \dots, A^{[N]}\}}{\operatorname{argmin}} \frac{\langle \Psi | H | \Psi \rangle}{\langle \Psi | \Psi \rangle}, \quad (\text{D10})$$

while keeping all tensors *outside* the unit-cell fixed. Sweeping from left to right, i.e. $i = 1 \dots N$, the minimization proceeds by optimizing one tensor $A^{[i]}$ at a time. For each site i , this minimization leads to a sparse eigenvalue equation with an effective Hamiltonian H_{eff} . For example, for the initial optimization of site $i = 1$, H_{eff} has the form

$$H_{eff} = \dots \begin{array}{ccccccc} \begin{bmatrix} \bigcirc \\ \bigcirc \end{bmatrix} & \begin{bmatrix} \bigcirc \\ \bigcirc \end{bmatrix} & \begin{bmatrix} \bigcirc \\ \bigcirc \end{bmatrix} & \begin{bmatrix} \bigcirc \\ \bigcirc \end{bmatrix} & \begin{bmatrix} \bigcirc \\ \bigcirc \end{bmatrix} & \begin{bmatrix} \bigcirc \\ \bigcirc \end{bmatrix} & \begin{bmatrix} \bigcirc \\ \bigcirc \end{bmatrix} \\ \begin{bmatrix} \bigcirc & \bigcirc \\ \bigcirc & \bigcirc \end{bmatrix} & \begin{bmatrix} \bigcirc & \bigcirc \\ \bigcirc & \bigcirc \end{bmatrix} & \begin{bmatrix} \bigcirc & \bigcirc \\ \bigcirc & \bigcirc \end{bmatrix} & \begin{bmatrix} \bigcirc & \bigcirc \\ \bigcirc & \bigcirc \end{bmatrix} & \begin{bmatrix} \bigcirc & \bigcirc \\ \bigcirc & \bigcirc \end{bmatrix} & \begin{bmatrix} \bigcirc & \bigcirc \\ \bigcirc & \bigcirc \end{bmatrix} & \begin{bmatrix} \bigcirc & \bigcirc \\ \bigcirc & \bigcirc \end{bmatrix} \\ \begin{bmatrix} \bigcirc \\ \bigcirc \end{bmatrix} & \begin{bmatrix} \bigcirc \\ \bigcirc \end{bmatrix} & \begin{bmatrix} \bigcirc \\ \bigcirc \end{bmatrix} & \begin{bmatrix} \bigcirc \\ \bigcirc \end{bmatrix} & \begin{bmatrix} \bigcirc \\ \bigcirc \end{bmatrix} & \begin{bmatrix} \bigcirc \\ \bigcirc \end{bmatrix} & \begin{bmatrix} \bigcirc \\ \bigcirc \end{bmatrix} \end{array} \dots \quad (\text{D11})$$

The unit-cell tensors are highlighted in red, and we have used a Matrix Product Operator representation² (see Appendix E below) of the Hamiltonian Eq.(46),

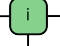
$$H = \dots \begin{array}{cccc} \begin{bmatrix} \bigcirc \\ \bigcirc \end{bmatrix} & \begin{bmatrix} \bigcirc \\ \bigcirc \end{bmatrix} & \begin{bmatrix} \bigcirc \\ \bigcirc \end{bmatrix} & \begin{bmatrix} \bigcirc \\ \bigcirc \end{bmatrix} \\ \begin{bmatrix} \bigcirc & \bigcirc \\ \bigcirc & \bigcirc \end{bmatrix} & \begin{bmatrix} \bigcirc & \bigcirc \\ \bigcirc & \bigcirc \end{bmatrix} & \begin{bmatrix} \bigcirc & \bigcirc \\ \bigcirc & \bigcirc \end{bmatrix} & \begin{bmatrix} \bigcirc & \bigcirc \\ \bigcirc & \bigcirc \end{bmatrix} \\ \begin{bmatrix} \bigcirc \\ \bigcirc \end{bmatrix} & \begin{bmatrix} \bigcirc \\ \bigcirc \end{bmatrix} & \begin{bmatrix} \bigcirc \\ \bigcirc \end{bmatrix} & \begin{bmatrix} \bigcirc \\ \bigcirc \end{bmatrix} \end{array} \dots \quad (\text{D12})$$

$C_{\alpha\beta}^{mn'} \equiv \begin{bmatrix} \bigcirc \\ \bigcirc \end{bmatrix}$ is a sparse four-leg tensor (see Appendix E below). Using standard contraction techniques for MPS (Appendix E) the infinite tensor network in Eq.(D11) can be contracted, resulting in the expression

$$H_{eff} = \begin{array}{ccccccc} \begin{bmatrix} \bigcirc \\ \bigcirc \end{bmatrix} & \begin{bmatrix} \bigcirc \\ \bigcirc \end{bmatrix} & \begin{bmatrix} \bigcirc \\ \bigcirc \end{bmatrix} & \begin{bmatrix} \bigcirc \\ \bigcirc \end{bmatrix} & \begin{bmatrix} \bigcirc \\ \bigcirc \end{bmatrix} & \begin{bmatrix} \bigcirc \\ \bigcirc \end{bmatrix} & \begin{bmatrix} \bigcirc \\ \bigcirc \end{bmatrix} \\ \begin{bmatrix} \bigcirc & \bigcirc \\ \bigcirc & \bigcirc \end{bmatrix} & \begin{bmatrix} \bigcirc & \bigcirc \\ \bigcirc & \bigcirc \end{bmatrix} & \begin{bmatrix} \bigcirc & \bigcirc \\ \bigcirc & \bigcirc \end{bmatrix} & \begin{bmatrix} \bigcirc & \bigcirc \\ \bigcirc & \bigcirc \end{bmatrix} & \begin{bmatrix} \bigcirc & \bigcirc \\ \bigcirc & \bigcirc \end{bmatrix} & \begin{bmatrix} \bigcirc & \bigcirc \\ \bigcirc & \bigcirc \end{bmatrix} & \begin{bmatrix} \bigcirc & \bigcirc \\ \bigcirc & \bigcirc \end{bmatrix} \\ \begin{bmatrix} \bigcirc \\ \bigcirc \end{bmatrix} & \begin{bmatrix} \bigcirc \\ \bigcirc \end{bmatrix} & \begin{bmatrix} \bigcirc \\ \bigcirc \end{bmatrix} & \begin{bmatrix} \bigcirc \\ \bigcirc \end{bmatrix} & \begin{bmatrix} \bigcirc \\ \bigcirc \end{bmatrix} & \begin{bmatrix} \bigcirc \\ \bigcirc \end{bmatrix} & \begin{bmatrix} \bigcirc \\ \bigcirc \end{bmatrix} \end{array} \quad (\text{D13})$$

We call $\begin{bmatrix} \bigcirc \\ \bigcirc \end{bmatrix}$ and $\begin{bmatrix} \bigcirc \\ \bigcirc \end{bmatrix}$ the effective left and right *unit-cell environments*. The labels indicate the index of the last

MPS tensor that has been contracted into $\left(4^0\right)$ and $\left(1^0\right)$.

The superscripts are the iDMRG iteration number. $\left(4^0\right)$ is thus the left environment of tensor $i = 1$ at iteration $q = 0$. (and likewise for $\left(1^0\right)$). An updated $\tilde{A}^{[i]} \equiv$  is obtained from the (properly reshaped and normalized) lowest eigen-vector of H_{eff} . Using a QR or SV decomposition, it is decomposed into

$$\left[\text{green square } i \right] = \left[\text{green triangle } i \right] \left[\text{green circle } \right] \quad (\text{D14})$$

and inserted back into the MPS. One then moves one site to the right, where the above procedure is repeated with

$$H_{eff} = \left(4^0\right) \left[\text{green } 1 \right] \left[\text{green } 2 \right] \left[\text{red } 3 \right] \left[\text{red } 4 \right] \left(1^0\right). \quad (\text{D15})$$

The tensors $\left(4^1\right)$ and $\left(3^1\right)$ are called the effective left and right environments of site $i = 2$. The optimization keeps sweeping right and left (using a similar update method for the left sweep) until sufficient convergence is reached (we only sweep once from left to right for our applications). The orthogonality center is then moved to the central bond, where a resolution of the identity $\left[\text{green } \bullet \right] \left[\text{red } \bullet \right]$ is inserted. The matrices $\left[\text{green } \bullet \right]$ are shifted to the left and right boundary of the unit-cell (see Fig. A3 (c) and (d)) where they are contracted into $\left[\text{pink } \bullet \right] = \left[\text{green } 4 \right] \left[\text{red } \bullet \right] \left[\text{green } 4 \right]$ (see Fig. A3 (a')). The state is now in a quasi-parallel decomposition with respect to a unit-cell that has been shifted by $N/2$. Note, however, that it is no longer in its canonical form. The next iteration consists of updating the tensors $\{\tilde{A}^{[N/2+1]}, \dots, \tilde{A}^{[N]}, \tilde{A}^{[1]}, \dots, \tilde{A}^{[N/2]}\}$ of this shifted unit-cell. To this end, one needs to calculate an effective Hamiltonian for the shifted unit-cell. Several slightly different methods can be used to proceed at this point. In the following, we will explain two of them in more detail.

In the iDMRG algorithm, the calculation of a new effective Hamiltonian is achieved by recycling the left and right unit-cell environments calculated during the previous iteration. The left and right unit-cell environments

at iteration $q = 1$, $\left(2^1\right)$ and $\left(3^1\right)$, in this case are given by

$$\left(2^1\right) = \left(4^0\right) \left[\text{green } 1 \right] \left[\text{green } 2 \right] \left(1^0\right) \quad (\text{D16})$$

$$\left(3^1\right) = \left[\text{green } 3 \right] \left[\text{green } 4 \right] \left(1^0\right), \quad (\text{D17})$$

The effective Hamiltonian for e.g. site $i = 3$ during the second iteration $q = 1$ assumes the form

$$H_{eff} = \left(2^1\right) \left[\text{pink } 3 \right] \left[\text{pink } 4 \right] \left[\text{pink } 1 \right] \left[\text{pink } 2 \right] \left(3^1\right). \quad (\text{D18})$$

We have here highlighted the currently optimized unit-cell tensors in pink. From here on the method proceeds by repeatedly cycling through the steps (b)-(a') of Fig. A3, and updating the left and right unit-cell environments as described above.

While this method works well in general, an inconsistency arises after the first iteration: the unit-cell environments in Eqs. (D16) and (D17) are calculated by adding updated tensors to $\left(4^0\right)$ and $\left(1^0\right)$. These two, however, have both been obtained from contracting an infinite tensor network containing the tensors of the *initial* MPS. They do not contain any information of the update and are thus different from the ones that would be obtained using the *current* MPS (which has been updated within each unit-cell). Thus, instead of recycling the environments after each iteration, one could also regauge the MPS into its canonical form and recalculate the effective left and right unit-cell environments. This approach is seen to result in slightly lower energies of the optimized MPS.

For the case of $N = 1$, a very similar approach has been proposed for the setting of homogeneous cMPS³², termed gradient optimization for cMPS. The gradient optimization for homogeneous lattices with $N = 1$ can be obtained by slightly tweaking the above method, as we will now describe in the following. Consider a state with $N = 1$ in its parallel decomposition, i.e.

$$|\Psi\rangle = \left[\text{green } 1 \right] \left[\text{red } \bullet \right] \left[\text{green } 1 \right] \left[\text{red } \bullet \right] \left[\text{green } 1 \right] \left[\text{red } \bullet \right]. \quad (\text{D19})$$

The effective unit-cell Hamiltonian for this state is given

by

$$H_{eff} = \cdots \begin{array}{c} \triangleleft \text{---} \text{---} \text{---} \triangleleft \\ | \quad | \quad | \\ \boxed{1} \quad \boxed{1} \quad \boxed{1} \\ | \quad | \quad | \\ \triangleleft \text{---} \text{---} \text{---} \triangleleft \end{array} \cdots = \begin{array}{c} \text{---} \text{---} \text{---} \\ | \quad | \quad | \\ \boxed{1} \quad \boxed{1} \quad \boxed{1} \\ | \quad | \quad | \\ \text{---} \text{---} \text{---} \end{array} \cdots \quad (\text{D20})$$

The update of the tensor $\triangleleft \text{---} \text{---} \text{---} \triangleleft$ proceeds now in a different manner than described above. Instead of finding an approximate lowest eigen-vector of Eq.(D20) we calculate a local gradient \star , with

$$\star \equiv \begin{array}{c} \triangleleft \text{---} \text{---} \text{---} \triangleleft \\ | \quad | \quad | \\ \boxed{1} \quad \boxed{1} \quad \boxed{1} \\ | \quad | \quad | \\ \triangleleft \text{---} \text{---} \text{---} \triangleleft \end{array}, \quad (\text{D21})$$

and use it to update the tensor:

$$\boxed{1} \equiv \triangleleft \text{---} \text{---} \text{---} \triangleleft - \alpha \star. \quad (\text{D22})$$

α is a small positive number. If α is chosen such as to minimize the energy expectation value

$$\begin{array}{c} \boxed{1} \\ | \\ \boxed{1} \quad \boxed{1} \quad \boxed{1} \\ | \\ \boxed{1} \end{array}, \quad (\text{D23})$$

the update is equivalent to finding the lowest energy state in the Krylov space spanned by $\{|\triangleleft \text{---} \text{---} \text{---} \triangleleft\rangle, |\star\rangle\}$. After this update, the state is in the form

$$|\Psi\rangle = \boxed{1} \square \boxed{1} \square \boxed{1} \square. \quad (\text{D24})$$

The matrices \square are now absorbed back into $\boxed{1}$ from the right hand side, and the iteration is restarted. A related approach for 1d lattice models which avoids the possibly ill-condition inversion \square has recently been proposed by Zauner-Stauber et al.⁴⁷. For the case of cMPS, the gradient optimization greatly outperforms other optimization approaches.

As we have found numerically, recalculating the full environments gives more accurate results for ground-state energies than recycling the environments. However, for large $N \gg 1$, it is slower than standard iDMRG due to the necessary recalculation of the environments. For the model considered in this manuscript, the difference in accuracy between the two approaches is small enough that

in present manuscript we use the simple recycling method for all calculations. In order to facilitate the extraction the cMPS content of the optimized lattice MPS, we use slightly modified techniques for shifting the orthogonality center and regauging the state, as described in detail in Appendix A.

Appendix E: Contracting Eq.(D11)

In this Appendix we discuss in detail how to contract the infinite tensor network appearing in Eq.(D11). In the following we discuss the case of a nearest neighbor Hamiltonian. The extension to more general Hamiltonians follows straightforwardly. Consider the case of a Hamiltonian of the form

$$H = \sum_{i \in \mathbb{Z}} h_{i,i+1} = \sum_{i \in \mathbb{Z}} \boxed{i \quad i+1}, \quad (\text{E1})$$

where we have introduced a diagrammatic notation for the two-site operators $h_{i,i+1}$. We assume further a periodicity of the Hamiltonian over $N = 4$ sites (see main text), such that we can decompose Eq.(E1) into

$$H = \sum_{j \in \mathbb{Z}} H_j \quad (\text{E2})$$

$$H_j = \sum_{i=1}^4 h_{i,i \oplus 1} = \sum_{i=1}^4 \boxed{i \quad i \oplus 1}, \quad (\text{E3})$$

with j running over the unit-cells, and $i \oplus 1 \equiv i \bmod N + 1$. Using standard techniques², H can be written in an MPO decomposition

$$H = \cdots \boxed{1} \boxed{2} \boxed{3} \boxed{4} \cdots, \quad (\text{E4})$$

where numbers label sites i inside the unit-cell. Horizontal lines denote auxiliary indices (with a bond-dimension M), and vertical lines are physical indices of the MPO. For example, for the Hamiltonian Eq.(46), a possible, non-unique MPO decomposition is given by

$$\boxed{i} = \begin{pmatrix} \mathbb{1} \\ c_i^\dagger \\ c_i \\ c_i^\dagger c_i \\ \mathcal{P}_i^0 \\ c_i^\dagger c_i \\ \mu_i c_i^\dagger c_i \quad \frac{-1}{2m\epsilon^2} c_i \quad \frac{-1}{2m\epsilon^2} c_i^\dagger \quad \frac{g}{\epsilon} c_i^\dagger c_i \quad \frac{1}{2m\epsilon^2} c_i^\dagger c_i \quad \frac{1}{2m\epsilon^2} \mathcal{P}_i^0 \quad \mathbb{1} \end{pmatrix}, \quad (\text{E5})$$

where we have only written entries different from 0. The MPO bond dimension is in this case $M = 7$. For later

reference we introduce the boundary MPO tensors

$$\begin{array}{|c|} \hline \mathbf{i} \\ \hline \end{array}, \quad \begin{array}{|c|} \hline \mathbf{i} \\ \hline \end{array}. \quad (\text{E6})$$

In our MPO convention, $\begin{array}{|c|} \hline \mathbf{i} \\ \hline \end{array}$ is given by the last column

of Eq.(E5), and $\begin{array}{|c|} \hline \mathbf{i} \\ \hline \end{array}$ is given by its first row. We refer the reader to the literature² for a detailed introduction to the MPO formalism.

Written out explicitly for the case $N = 4$ we have

$$\sum_{i=1}^4 h_{i,i\oplus 1} = \begin{array}{c} \begin{array}{cccc} \bullet & \bullet & \bullet & \bullet \\ 1 & 2 & 3 & 4 & 1 \end{array} \\ \begin{array}{|c|} \hline 1 & 2 \\ \hline \end{array} \\ + \\ \begin{array}{|c|} \hline 2 & 3 \\ \hline \end{array} \\ + \\ \begin{array}{|c|} \hline 3 & 4 \\ \hline \end{array} \\ + \\ \begin{array}{|c|} \hline 4 & 1 \\ \hline \end{array} \end{array}. \quad (\text{E7})$$

For a fixed unit-cell we will now calculate the right unit-cell environment (see main text)

$$\begin{array}{|c|} \hline \mathbf{1} \\ \hline \end{array} \equiv \begin{array}{|c|} \hline \begin{array}{cccc} \triangleleft 1 & \triangleleft 2 & \triangleleft 3 & \triangleleft 4 \\ \hline \mathbf{1} & \mathbf{2} & \mathbf{3} & \mathbf{4} \\ \hline \triangleleft 1 & \triangleleft 2 & \triangleleft 3 & \triangleleft 4 \end{array} \\ \hline \end{array} \dots \quad (\text{E8})$$

For an MPO with e.g. bond dimension M , this would be a vector of $M D \times D$ matrices. In vector notation, it is

$$\begin{pmatrix} \begin{array}{|c|} \hline \mathbf{1} \\ \hline \end{array} \\ \vdots \\ \begin{array}{|c|} \hline \mathbf{M} \\ \hline \end{array} \end{pmatrix} = \begin{pmatrix} \begin{array}{c} \begin{array}{|c|} \hline \mathbf{1} \\ \hline \end{array} \\ \vdots \\ \begin{array}{|c|} \hline \mathbf{M-1} \\ \hline \end{array} \\ \vdots \\ \begin{array}{|c|} \hline \mathbf{1} \\ \hline \end{array} \end{array} \\ \begin{array}{c} \begin{array}{|c|} \hline \triangleleft 1 & \triangleleft 2 & \triangleleft 3 & \triangleleft 4 \\ \hline \mathbf{1} & \mathbf{2} & \mathbf{3} & \mathbf{4} \\ \hline \triangleleft 1 & \triangleleft 2 & \triangleleft 3 & \triangleleft 4 \end{array} \\ + \\ \begin{array}{|c|} \hline \mathbf{1} & \mathbf{2} \\ \hline \end{array} \\ + \\ \begin{array}{|c|} \hline \mathbf{2} & \mathbf{3} \\ \hline \end{array} \\ + \\ \begin{array}{|c|} \hline \mathbf{3} & \mathbf{4} \\ \hline \end{array} \\ + \\ \begin{array}{|c|} \hline \mathbf{4} & \mathbf{1} \\ \hline \end{array} \\ \vdots \\ \begin{array}{|c|} \hline \triangleleft 1 & \triangleleft 2 & \triangleleft 3 & \triangleleft 4 \\ \hline \mathbf{M-1} & \mathbf{M} & \mathbf{1} & \mathbf{2} \\ \hline \triangleleft 1 & \triangleleft 2 & \triangleleft 3 & \triangleleft 4 \end{array} \end{array} \end{pmatrix}, \quad (\text{E9})$$

where we have explicitly written out the vector index. Using an MPO decomposition of the unit-cell Hamiltonian,

$$\begin{array}{|c|} \hline 1 & 2 \\ \hline \end{array} + \begin{array}{|c|} \hline 2 & 3 \\ \hline \end{array} + \begin{array}{|c|} \hline 3 & 4 \\ \hline \end{array} + \begin{array}{|c|} \hline 4 & 1 \\ \hline \end{array} = \begin{array}{|c|} \hline \mathbf{1} & \mathbf{2} & \mathbf{3} & \mathbf{4} \\ \hline \end{array} \begin{array}{|c|} \hline \mathbf{1} \\ \hline \end{array}, \quad (\text{E10})$$

we can rewrite the last component of Eq.(E24) as

$$\left(\sum_{n=0}^{\infty} \left[\begin{array}{|c|} \hline \triangleleft 1 & \triangleleft 2 & \triangleleft 3 & \triangleleft 4 \\ \hline \mathbf{1} & \mathbf{2} & \mathbf{3} & \mathbf{4} \\ \hline \triangleleft 1 & \triangleleft 2 & \triangleleft 3 & \triangleleft 4 \end{array} \right]^n \begin{array}{|c|} \hline \mathbf{1} & \mathbf{2} & \mathbf{3} & \mathbf{4} \\ \hline \end{array} \begin{array}{|c|} \hline \mathbf{1} \\ \hline \end{array} \right) \quad (\text{E11})$$

with the right-normalized unit-cell transfer operator

$$\mathbb{E}_r \equiv \begin{array}{|c|} \hline \triangleleft 1 & \triangleleft 2 & \triangleleft 3 & \triangleleft 4 \\ \hline \mathbf{1} & \mathbf{2} & \mathbf{3} & \mathbf{4} \\ \hline \triangleleft 1 & \triangleleft 2 & \triangleleft 3 & \triangleleft 4 \end{array}. \quad (\text{E12})$$

and the renormalized unit-cell Hamiltonian

$$|h_r\rangle \equiv \begin{array}{|c|} \hline \triangleleft 1 & \triangleleft 2 & \triangleleft 3 & \triangleleft 4 \\ \hline \mathbf{1} & \mathbf{2} & \mathbf{3} & \mathbf{4} \\ \hline \triangleleft 1 & \triangleleft 2 & \triangleleft 3 & \triangleleft 4 \end{array} \begin{array}{|c|} \hline \mathbf{1} \\ \hline \end{array}. \quad (\text{E13})$$

The operator \mathbb{E}_r has a left and right dominant eigenvector $\langle l |, |\mathbb{1}\rangle$ to eigenvalue $\eta = 1$. Thus, the geometric series in Eq.(E11) diverges. This can be cured by restricting the operator \mathbb{E}_r to the orthogonal complement of the subspace $|\mathbb{1}\rangle \langle l|$, i.e. by the replacements

$$\mathbb{E}_r \rightarrow \mathbb{E}_{r\perp} = \mathbb{E}_r - |\mathbb{1}\rangle \langle l| \quad (\text{E14})$$

$$|h_r\rangle \rightarrow |h_{r\perp}\rangle = |h_r\rangle - \langle l|h_r\rangle |\mathbb{1}\rangle \quad (\text{E15})$$

The geometric series Eq.(E11) transforms into

$$|H_r\rangle_{\perp} \equiv \left(\sum_{n=0}^{\infty} [\mathbb{E}_{r\perp}]^n \right) |h_{r\perp}\rangle_{\perp} = \frac{1}{\mathbb{1} - \mathbb{E}_{r\perp}} |h_{r\perp}\rangle_{\perp} \quad (\text{E16})$$

which can be solved iteratively for $|H_r\rangle_{\perp}$ using sparse solvers like e.g. the *lgmres* method from the *scipy* package.

The approach for calculating the left unit-cell environment starts from the expression

$$\begin{array}{|c|} \hline \triangleleft 4 & \triangleleft 1 & \triangleleft 2 & \triangleleft 3 & \triangleleft 4 \\ \hline \mathbf{3} & \mathbf{4} & \mathbf{3} & \mathbf{4} & \mathbf{3} & \mathbf{4} \\ \hline \mathbf{2} & \mathbf{3} & \mathbf{2} & \mathbf{3} & \mathbf{2} & \mathbf{3} \\ \hline \mathbf{1} & \mathbf{2} & \mathbf{1} & \mathbf{2} & \mathbf{1} & \mathbf{2} \\ \hline \mathbf{4} & \mathbf{1} & \mathbf{4} & \mathbf{1} & \mathbf{4} & \mathbf{1} \\ \hline \triangleleft 4 & \triangleleft 1 & \triangleleft 2 & \triangleleft 3 & \triangleleft 4 \\ \hline \end{array} \quad (\text{E17})$$

and then follows the same steps, using an MPO decomposition for the unit-cell Hamiltonian of the form

$$\begin{array}{|c|} \hline \mathbf{4} & \mathbf{1} \\ \hline \end{array} + \begin{array}{|c|} \hline \mathbf{1} & \mathbf{2} \\ \hline \end{array} + \begin{array}{|c|} \hline \mathbf{2} & \mathbf{3} \\ \hline \end{array} + \begin{array}{|c|} \hline \mathbf{3} & \mathbf{4} \\ \hline \end{array} = \begin{array}{|c|} \hline \mathbf{4} & \mathbf{1} & \mathbf{2} & \mathbf{3} & \mathbf{4} \\ \hline \end{array}. \quad (\text{E18})$$

With the definitions

$$\mathbb{E}_l \equiv \begin{array}{c} \begin{array}{cccc} \triangleleft 1 & \triangleleft 2 & \triangleleft 3 & \triangleleft 4 \\ \vdots & \vdots & \vdots & \vdots \\ \triangleleft 1 & \triangleleft 2 & \triangleleft 3 & \triangleleft 4 \end{array} \\ \text{(E19)} \end{array}$$

$$\langle h_l | \equiv \begin{array}{c} \begin{array}{cccc} \triangleleft 4 & \triangleleft 1 & \triangleleft 2 & \triangleleft 3 & \triangleleft 4 \\ \textcircled{4} & \textcircled{1} & \textcircled{2} & \textcircled{3} & \textcircled{4} \\ \triangleleft 4 & \triangleleft 1 & \triangleleft 2 & \triangleleft 3 & \triangleleft 4 \end{array} \\ \text{(E20)} \end{array}$$

and the replacements

$$\mathbb{E}_l \rightarrow \mathbb{E}_{l\perp} = \mathbb{E}_l - |r\rangle \langle \mathbb{1}| \quad \text{(E21)}$$

$$\langle h_l | \rightarrow \langle h_l |_{\perp} = \langle h_l | - \langle h_l | r \rangle \langle \mathbb{1}| \quad \text{(E22)}$$

one obtains

$$\langle H_l |_{\perp} \equiv \langle h_l |_{\perp} \frac{1}{\mathbb{1} - \mathbb{E}_{l\perp}}. \quad \text{(E23)}$$

Here, $\langle \mathbb{1}|$ and $|r\rangle$ are the dominant left and right eigen-

vectors of \mathbb{E}_l . The final result is

$$\begin{array}{c} \textcircled{1} = \left(\begin{array}{c} \begin{array}{c} \triangleleft 4 \\ \vdots \\ \triangleleft 1 \end{array} \\ \textcircled{1} \\ \begin{array}{c} \triangleleft 1 \\ \vdots \\ \triangleleft 4 \end{array} \\ |H_r\rangle_{\perp} \end{array} \right) \quad \text{(E24)} \end{array}$$

$$\textcircled{4} = \left(\langle H_l |_{\perp}, \begin{array}{c} \triangleleft 4 \\ \vdots \\ \triangleleft 4 \end{array} \textcircled{4}^{-2}, \dots, \begin{array}{c} \triangleleft 4 \\ \vdots \\ \triangleleft 4 \end{array} \textcircled{4}^{-M} \right) \quad \text{(E25)}$$